9-24-2022

Single-cell RNA transcriptome analysis of CNS immune cells reveals CXCL16/CXCR6 as maintenance factors for tissue-resident T cells that drive synapse elimination

Sarah F Rosen

Allison L Soung

Wei Yang

Shenjian Ai

Marlene Kanmogne

See next page for additional authors

Authors

Sarah F Rosen, Allison L Soung, Wei Yang, Shenjian Ai, Marlene Kanmogne, Veronica A Davé, Maxim Artyomov, Jeffrey A Magee, and Robyn S Klein

Single-cell RNA transcriptome analysis of CNS immune cells reveals CXCL16/CXCR6 as maintenance factors for tissue-resident T cells that drive synapse elimination

Sarah F. Rosen[1,2†], Allison L. Soung[1,2†], Wei Yang[3], Shenjian Ai[1,2], Marlene Kanmogne[1,2], Veronica A. Davé[1,2], Maxim Artyomov[4], Jeffrey A. Magee[2,3,4,5] and Robyn S. Klein[1,2,4,6*]

Abstract

Background: Emerging RNA viruses that target the central nervous system (CNS) lead to cognitive sequelae in survivors. Studies in humans and mice infected with West Nile virus (WNV), a re-emerging RNA virus associated with learning and memory deficits, revealed microglial-mediated synapse elimination within the hippocampus. Moreover, CNS-resident memory T (T_RM) cells activate microglia, limiting synapse recovery and inducing spatial learning defects in WNV-recovered mice. The signals involved in T cell-microglia interactions are unknown.

Methods: Here, we examined immune cells within the murine WNV-recovered forebrain using single-cell RNA sequencing to identify putative ligand-receptor pairs involved in intercellular communication between T cells and microglia. Clustering and differential gene analyses were followed by protein validation and genetic and antibody-based approaches utilizing an established murine model of WNV recovery in which microglia and complement promote ongoing hippocampal synaptic loss.

Results: Profiling of host transcriptome immune cells at 25 days post-infection in mice revealed a shift in fore-brain homeostatic microglia to activated subpopulations with transcriptional signatures that have previously been observed in studies of neurodegenerative diseases. Importantly, CXCL16/CXCR6, a chemokine signaling pathway involved in T_RM cell biology, was identified as critically regulating CXCR6 expressing CD8$^+$ T_RM cell numbers within the WNV-recovered forebrain. We demonstrate that CXCL16 is highly expressed by all myeloid cells, and its unique receptor, CXCR6, is highly expressed on all CD8$^+$ T cells. Using genetic and pharmacological approaches, we demonstrate that CXCL16/CXCR6 not only is required for the maintenance of WNV-specific CD8 T_RM cells in the post-infectious CNS, but also contributes to their expression of T_RM cell markers. Moreover, CXCR6$^+$CD8$^+$ T cells are required for glial activation and ongoing synapse elimination.

†Sarah F. Rosen and Allison L. Soung have equal contributions.

*Correspondence: rklein@wustl.edu

[6] Department of Neuroscience, Washington University School of Medicine, St. Louis, MO, USA
Full list of author information is available at the end of the article

Rosen *et al. Genome Medicine* (2022) 14:108

Page 2 of 20

Conclusions: We provide a comprehensive assessment of the role of CXCL16/CXCR6 as an interaction link between microglia and CD8$^+$ T cells that maintains forebrain T$_R$M cells, microglial and astrocyte activation, and ongoing synapse elimination in virally recovered animals. We also show that therapeutic targeting of CXCL16 in mice during recovery may reduce CNS CD8$^+$ T$_R$M cells.

Background

Neurotropic viruses may trigger the onset of neurodegenerative processes in the central nervous system (CNS) that lead to progressive memory impairments. West Nile virus (WNV) is an emerging neurotropic flavivirus that is the leading cause of domestically acquired arboviral disease and epidemic encephalitis in the USA [1]. Acute symptomatic syndromes include a self-limited febrile illness, West Nile fever (WNF), while more severe neuroinvasive diseases include meningitis, encephalitis, or flaccid paralysis. Ninety percent of patients with West Nile virus neuroinvasive disease (WNND) survive their acute illness due to the effector functions of antiviral T cells that clear the virus in the CNS, predominantly via noncytolytic cytokines, such as interferon (IFN)-γ [2–4]. The majority of these patients, however, develop debilitating cognitive and memory impairments that persist and worsen for years after recovery from encephalitis [5]. The mechanisms by which WNV infection in the CNS leads to long-term cognitive sequelae remain largely unknown.

Memory formation and consolidation is the result of complex circuitry between the hippocampus and cortex. The Cornu Ammoni (CA)3 region of the dorsal hippocampus, in particular, plays an important role in the formation of spatial memories in rodents [6–8]. Using a novel murine model of WNV recovery, we previously traced spatial learning deficits to microglial engulfment of presynaptic terminals in the CA3 region of the hippocampus, acutely and ongoing, and is driven by classical complement protein C1qA expressed by neurons and microglia [9]. We also showed that CD8$^+$IFNγ$^+$ T cells that persist in the CNS as resident memory T (T$_R$M) cells are the most proximal trigger of microglial activation, synapse elimination, and spatial learning deficits during viral recovery [10]. The factors that determine which CD8$^+$ T cells persist, how they interact with distinct CNS myeloid subsets, and whether this contributes to synapse elimination or cognitive impairment are not known.

To advance the discovery of cellular and molecular mechanisms that regulate differentiation and retention of CNS CD8$^+$ T$_R$M, we searched for genetic signatures of myeloid subpopulations and putative ligand-receptor regulators of microglia-T cell interactions, employing single-cell RNA sequencing (scRNA-seq) on forebrain immune cells (cortex and hippocampus) derived from WNV-recovered mice. Profiling of host transcriptome at 25 days post-infection revealed a shift in forebrain homeostatic microglia to activated subpopulations with transcriptional signatures similar to those previously observed in studies of neurodegenerative diseases [11–14]. Focusing on microglia and T cell subpopulations, selected genomic results underwent in vivo protein validation, followed by in vivo functional studies to define mechanisms that drive their interactions and functions.

Of the possible ligand-receptor pairs that drive intercellular interactions, cell localization, and differentiation, chemokine signaling pathways are likely candidates. These molecules regulate the migration and recruitment of T cells during homeostasis and into inflamed tissues, where they also promote their differentiation [15, 16]. We identified *Cxcr6* as the only chemokine receptor in the top 20 differentially expressed genes (DEGs) within the CD8$^+$ T cell cluster. CXCR6 is the unique receptor for the transmembrane chemokine CXCL16 [17]; consistent with this, *Cxcl16* was highly expressed in all of the myeloid cell populations in the WNV-recovered CNS. CXCL16 is synthesized as a transmembrane multidomain molecule, with a soluble version generated by cleavage of the transmembrane form through the actions of cell-surface proteases, such as a disintegrin and metalloproteinase (ADAM) 10 and 17 [18–20]. CXCL16 is expressed in low levels by microglia during homeostatic conditions and is highly expressed in the brain during pathological conditions such as multiple sclerosis, glioma, schwannomas, and meningiomas [19, 21–25]. CXCR6 has been shown to play an important role in the localization and retention of T$_R$M cells in the liver and lungs after viral infection [26–28]. Within the CNS, T$_R$M cells that populate the human brain express CXCR6 [29], and meningeal γδ T cells have been shown to express high levels of CXCR6 [30].

Using *Cxcr6*$^{-/-}$ mice and antibody-based neutralization of CXCL16, we demonstrate that CXCL16/CXCR6 are maintenance and differentiation factors for CD8$^+$ T$_R$M cells in the forebrain of WNV-recovered mice. Furthermore, CXCR6 signaling promotes microglial activation and astrocytic interleukin (IL)-1β production, leading to ongoing synapse elimination in the CA3 region of the hippocampus. We provide novel genomic evidence for virus-mediated differentiation of neuropathologic microglial subsets and the causal role of CXCL16/CXCR6 in hippocampal pathology during recovery from

Rosen *et al. Genome Medicine*   (2022) 14:108

Page 3 of 20

WNV CNS infection. We also provide evidence that targeting this pathway may be a successful approach for the prevention of microglial-mediated synapse loss that occurs after recovery from flavivirus encephalitis.

Methods
Mice
Eight to 10-week-old male and female mice were used for all experiments. C57BL/6J mice and *Cxcr6*$^{-/-}$ and *Cd8*$^{-/-}$ mice were obtained from Jackson Laboratories. Transgenic mice were backcrossed more than ten generations to C57BL/6 mice at Jackson Laboratories. Eight to 10-week-old male and female mice were used for all experiments. C57BL/6J mice and Cxcr6−/− and Cd8−/−mice were obtained from Jackson Laboratories. Transgenic mice were backcrossed more than ten generations to C57BL/6J at Jackson Laboratories. For viral inoculations as well as euthanasia, mice were anesthetized with a cocktail of ketamine/xylazine/acepromazine. All experiments followed guidelines approved by the Washington University School of Medicine Animals Safety Committee (IACUC Animal Welfare Assurance # A-3381-01, protocol no. 20180120).

Mouse model of WNV infection
M. Diamond at Washington University in St. Louis provided the WNV-NS5-E218A strain utilized for intracranial infections. WNV-NS5-E218A contains a single point mutation in the gene encoding 2′-O-methyltransferase. Deeply anesthetized mice were intracranially administered 1×10^4 plaque-forming units (p.f.u.) of WNV-NS5-E218A into the third ventricle of the brain with a guided 29-gauge needle. Viruses were diluted in 10μl of 0.5% fetal bovine serum in Hank's balanced salt solution (HBBS, Gibco). Mock-infected mice were intracranially injected with viral diluent.

scRNA-seq
Mice (2 groups, *n*=2 per group, 4 mice pooled per *n*) were deeply anesthetized and perfused intracardially with ice-cold dPBS (Gibco). Forebrain tissue was aseptically dissected, minced, and enzymatically digested in HBSS (Gibco) containing collagenase D (Sigma, 50mg/ml), TLCK trypsin inhibitor (Sigma, 100μg/ml), DNase I (Sigma, 100U/μl), and HEPES 7.2 (Gibco, 1M), for 1h at 37°C while shaking. The tissue was pushed through a 70-μm strainer and spun down at 500*g* for 10min. To remove myelin debris, cells were resuspended in 37% Percoll and spun at 1200g for 30min. To minimize cell loss and aggregation, cells were resuspended at 100 cells/μL in PBS containing 0.04% (w/v) BSA. ~17,500 cells were partitioned into nanoliter-scale Gel Bead-In-EMulsions

(GEMs) to achieve single-cell resolution for a maximum of 10,000 individual cells/sample. Poly-adenylated mRNA from an individual cell was tagged with a unique 16 basepair 10x barcode and 10 basepair unique molecular identifier utilizing the v2 Chromium Single Cell 3′ Library Kit and Chromium instrument (10x Genomics). Full-length cDNA was amplified to generate sufficient mass for library construction. cDNA amplicon size (~400 basepair) for the library was optimized using enzymatic fragmentation and size selection. The final library was sequence-ready and contained four unique sample indexes. The concentration of the 10x single cell library was determined via qPCR (Kapa Biosystems). The libraries were normalized, pooled, and sequenced on the HiSeq4000 platform (Illumina). Four single-cell libraries were sequenced across an entire HiSeq4000 flow cell targeting ~45,000 reads per cell.

Alignment and barcode assignment
The Cell Ranger Single-Cell Software Suite was utilized to perform sample demultiplexing, barcode processing, and single-cell 3′ counting. Cellranger mkfastq was used to demultiplex raw base call files from the HiSeq4000 sequencer into sample-specific fastq files. Files were demultiplexed with 98%$^+$ perfect barcode match and 74%$^+$ q30 reads. To align reads to the mm10 mouse genome, fastq files for each sample were processed with cellranger counts. Samples were subsampled to have equal numbers of confidently mapped reads per cell. Four thousand one hundred thirty-two total cells were counted after filtration and cluster removal.

Preprocessing analysis with Seurat package
The Seurat package was used to analyze the processed scRNA data. Filtered genes by barcode expression matrices from Cell Ranger were used as analysis inputs. The merge function was used to pool samples. For quality control (QC), cells that expressed genes lower than 300 or higher than 4000 and those with more than 5% reads from mitochondrial genes were removed. The reads were log normalized with a scale factor of 10,000 and the percentage of mitochondrial reads regressed out using the Seurat R package. The QC plots of the remaining cells that were analyzed showing the distribution of total reads per cell (ncount_RNA) and numbers of genes expressed per cell (nFeature_RNA) are provided in Additional file 1: Fig. S1b.

Dimensionality reduction and clustering
The Seurat FindVariableGenes function was used to identify the most variable genes, which were then used for dimension reduction using PCA analysis. t-distributed Stochastic Neighbor Embedding (T-SNE) plots were used to visualize cells. For clustering, we used FindClusters

Rosen *et al. Genome Medicine* (2022) 14:108

Page 4 of 20

that utilizes shared nearest neighbors (SNN) and modularity optimization. This is based off the clustering algorithm with 20 PCA components and a clustering resolution of 0.3.

Identification of cluster-specific genes and marker-based classification

The Seurat FindAllMarkers function was used with the default Wilcoxon rank sum test for single-cell gene expression to identify marker genes. For each cluster, only genes that were expressed in more than 35% of cells with at least 0.25-fold difference were considered. Major CNS cell-type identities for each cluster were assigned by cross-referencing these genes with published gene expression datasets [31–35]. Differential expression tests between clusters were performed using the FindMarkers function using the Wilcoxon rank sum test, with significant genes identified as with adjusted P values ≤ 0.05.

Microglial cluster analysis

After assigning cell-type identities to the clusters, differential expression tests were performed comparing clusters 0 (homeostatic microglia), 1 (activated microglia-1), and 3 (activated microglia-2) with the Seurat findMarkers function using the default options and Wilcoxon rank sum test.

Pathway analysis

Generally applicable gene set enrichment (GAGE) method was used [36] based on the log2 fold changes from the single-cell differential expression analysis.

Flow cytometry

Murine forebrain cells were isolated and stained with fluorescence-conjugated antibodies. Briefly, mice were anesthetized and perfused with ice-cold dPBS (Gibco). Forebrain tissue was dissected out, minced, and enzymatically digested at 37℃ for 1h with shaking. The digestion buffer contained collagenase D (Sigma, 50mg/ml), TLCK trypsin inhibitor (Sigma, 100μg/ml), DNase I (Sigma, 100U/μl), HEPES buffer, and pH7.2 (Gibco, 1M) in HBSS (Gibco). The tissue was then pushed through a 70-μm strainer and pelleted by a 500g spin cycle for 10min. Cells were resuspended in 37% Percoll and spun at 1200g for 30min to remove myelin debris and then resuspended in FACS buffer. Cells were blocked for 5min at 4℃ with TruStain fcX (BioLegend, cat. no. 101320), followed by cell surface staining for 15min at 4℃ and cell fixation/permeabilization for 30min at 4℃. Cells were blocked again for 10min at room temperature followed by intracellular staining for 10min at room temperature and resuspended in 2% PFA for data acquisition. Data were collected using a Fortessa X-20 instrument and analyzed with the software FlowJo.

Antibodies for flow cytometry

The following antibodies were used for flow cytometry: CD11b (Brilliant Violet 605, BioLegend, cat. no. 101257), CD103 (APC/Cy7, BioLegend, cat. no. 121432), CD4 (APC, BioLegend, cat. no. 100411), CD45 (PerCP/Cy5.5, BioLegend, cat. no. 103132), CD8 (Brilliant Violet 711, BioLegend, cat. no. 100748), CXCR6 (PE, BioLegend, cat. no. 151103), Foxp3 (PerCP-Cy5.5, Biosciences, cat. no 563902), GFP (AF488, BioLegend, cat. no. 338008), and I-A/I-E (MHC-II, APC/Cy7, BioLegend, cat. no. 107628), CD103 (Brilliant Violet 605, BioLegend, cat. no. 121433), CD69 (Brilliant Violet 421, BD Biosciences, cat. no. 562920), CD45 (BV737, BD Biosciences, cat. no. 748371), and LIVE/DEAD fixable blue dead cell stain kit (Invitrogen, cat. no. L23105).

CD8$^+$ T cell adoptive transfer

Spleens harvested (using the aseptic technique) from naïve C57BL/6J or *Cxcr6$^{-/-}$* mice were placed in sterile, ice-cold RPM1-1640 medium (Sigma) with 10% fetal bovine serum (FBS, Gibco). Cells were then strained into a single-cell suspension. After centrifugation (500g for 5min at 4℃), red blood cells were lysed in ACK lysis buffer (Gibco) on ice for 5min. Cells were diluted with RPMI/FBS buffer and centrifuged again. CD8$^+$ T cells were isolated using a negative selection CD8a$^+$ T cell isolation kit (mouse, Miltenyi, cat. no. 130-095-236). CD8$^+$ (4×10^6 cells) were injected intravenously (i.v.) (0.2 ml) into male *Cd8$^{-/-}$* mice.

Immunohistochemistry (IHC)

Mice were anesthetized and perfused with ice-cold dPBS (Gibco), followed by ice-cold 4% paraformaldehyde (PFA). Brains were post-fixed overnight in 4% PFA and then cryopreserved in 30% sucrose (three exchanges every 24h). Prior to tissue sectioning (10 μm), samples were frozen in OCT compound (Fischer). Tissue sections were washed with PBS and permeabilized with 0.1–0.3% Triton X-100 (Sigma-Aldrich) and blocked with 5% normal goat serum (Sigma-Aldrich) at room temperature for 1h. Slides were then incubated in primary antibody overnight at 4℃. Slides were then incubated in secondary antibodies at room temperature for 1h, and nuclei were counterstained with 4,6-diamidino-2-phenylindole (DAPI; Invitrogen). ProLong Gold Antifade Mountant (Thermo Fisher) was applied on slides prior to coverslips. A Zeiss LSM 880 confocal laser scanning microscope and software from Zeiss were used to acquire images. Immunofluorescent signals were quantified using the software ImageJ.

Rosen *et al. Genome Medicine* (2022) 14:108

Page 5 of 20

RNAscope in situ hybridization (ISH/IHC)

Mice were anesthetized and perfused with ice-cold dPBS (Gibco) and post-fixed overnight in 4% PFA. Brains were then cryopreserved in 30% sucrose (three exchanges every 24h) and embedded in OCT compound (Fischer). Ten-micrometer sagittal tissue sections were prepared. RNAscope 2.5 HD Assay-Red (ACD, cat. No. 322360) was performed as per the manufacturer's instructions. A probe against CXCL16 mRNA (ACD) was used. For ISH/IHC experiments, IHC procedures, as previously described, followed ISH probe detection. Images were acquired using a Zeiss LSM 880 confocal laser scanning microscope and processed using software from Zeiss. Immunofluorescent signals were quantified using the software ImageJ.

Antibodies for immunohistochemistry

The following primary antibodies were used for IHC analyses: CD3 (1:200, BD Sciences, cat. no. 556970), GFAP (1:250; Thermo, cat. no. 13–0300, clone 2.2B10), GFP (1:200, abcam, cat. no. ab13970), IBA1 (1:200, Synaptic Systems, cat. no. 234 006), IL-1β (1:100; R&D, cat. no. AF-401), synaptophysin (1:250; Synaptic Systems, cat. no. 101004, polyclonal), and C1q (1:200; Abcam, cat. No. ab182451, monoclonal). Secondary antibodies conjugated to Alexa-488 (Invitrogen, cat. no. A21206) or Alexa-555 (Invitrogen, cat. no. A21435) were used at a 1:200 dilution.

Measurement of viral burden

Mice were infected with WNV and euthanized at specific days post-infection, as indicated. For tissue collection, mice were deeply anesthetized, and the brain was removed and micro-dissected. All tissues collected were weighed and then homogenized with zirconia beads in a MagNA Lyser instrument (Roche Life Science) in 500μl of PBS and stored at −80°C until virus titration. Thawed samples were clarified by centrifugation (2000g at 4°C for 10min) and then diluted serially before infection of BHK21 cells. Plaque assays were overlaid with low-melting point agarose, fixed 4 days later with 10% formaldehyde, and stained with crystal violet. The viral burden was expressed on a log10 scale as p.f.u. per gram of tissue.

Anti-CXCL16 treatment

Monoclonal rat IgG$_{2A}$ CXCL16 neutralizing antibody (R&D Systems, Clone # 142417, cat. no. MAB503) or monoclonal Rat IgG$_{2A}$ isotype control (R&D Systems, Clone # 54447 cat. no. MAB006) was administered via retro-orbital injection at a dose of 25μg for 4 consecutive days on days 7, 8, 9, and 10 post-infection. Optimal dosage and time points were chosen based off pilot experiments (Additional file 1: Fig. S8).

CXCL16 ELISA measurement

Tissues were collected in a complete extraction buffer on ice and homogenized with an electric homogenizer. Complete extraction buffer was made of 100 mM Tris, pH7.4 (Gibco), 150mM NaCl (Gibco), 1mM EGTA (Gibco), 1mM EDTA (Gibco), 1% Triton X-100 (Sigma-Aldrich), 0.5% Sodium deoxycholate (Thermo Scientific), and protease and phosphatase inhibitor (78440, Thermo Scientific). Samples were centrifuged for 20min at 13,000rpm at 4°C. The level of CXCL16 was detected using a commercial ELISA kit (DY503, R&D Systems, Inc., MN, USA), according to the manufacturer's guidelines. The OD values at wavelengths of 450 nm and 540 nm were measured by a microplate reader. Readings at 540 nm were subtracted from those of readings at 450 nm for wavelength correction. Concentrations of CXCL16 were calculated on the basis of a standard curve.
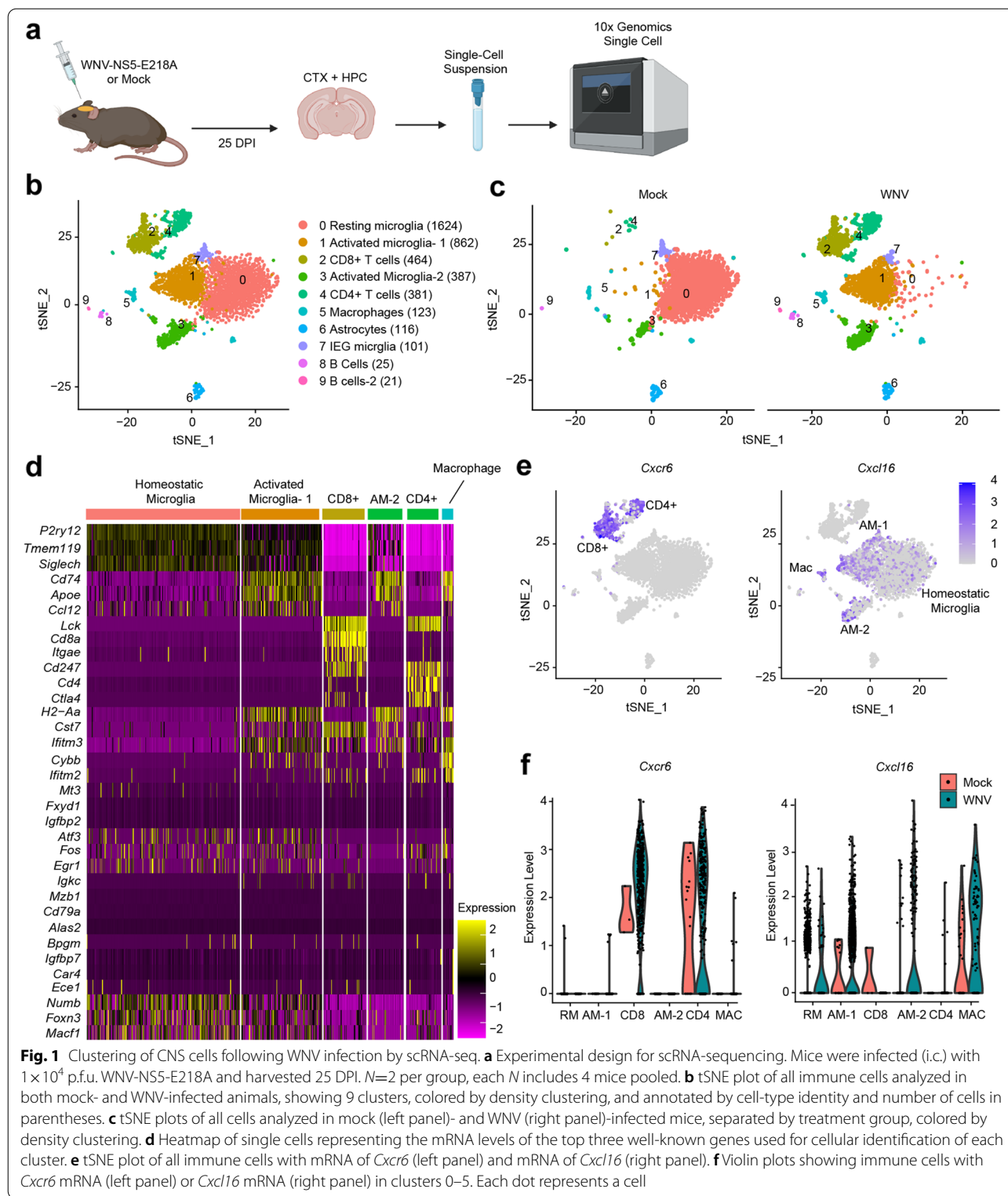
Statistical analysis

Prism 7.0 (GraphPad Software) was used to perform statistical analyses. All data were analyzed using an unpaired Student's *t*-test and one-way or two-way ANOVA and corrected for multiple comparisons as indicated in the corresponding figure legends. A *P* value of $\leq$ 0.05 was considered significant.

Results

scRNA-seq analysis identified nine major cellular subtypes present in the WNV-recovered CNS

To investigate the responses of myeloid cell subpopulations and T cells after recovery from viral encephalitis and determine whether they share similar transcriptional signatures to those seen in neurodegenerative diseases in an unbiased manner, we performed scRNA-seq analyses on forebrain tissues (cortices and hippocampi) collected from C57BL/6 mock- and WNV-infected mice at 25 days post-infection (DPI) (Fig. 1a). We deliberately chose cell isolation methods that would enrich for myeloid and T cell populations without altering their activation status or transcriptional profile signature [37, 38] at the expense of isolation of neural cell types, which were not the focus of our study. These studies used an established model of WNND, in which mice are infected intracranially with 10^4 plaque-forming units (PFU) of an attenuated strain of WNV, WNV-NS5-E218A, which contains a single point mutation in the gene encoding 2′-O-methyltransferase, leading to type I interferon-mediated viral clearance by 15 DPI and 90% survival [9]. Forebrain tissue was collected for analysis as these brain regions are sites of processes that regulate learning and memory [6–10]. A single-cell suspension with an ~95% live cell outcome (Additional file 1: Fig. S1c) was prepared from dissociated CNS tissue and after strict quality control transcriptomes

Rosen *et al. Genome Medicine*   (2022) 14:108

Page 6 of 20

Fig. 1 Clustering of CNS cells following WNV infection by scRNA-seq. **a** Experimental design for scRNA-sequencing. Mice were infected (i.c.) with 1×10^4 p.f.u. WNV-NS5-E218A and harvested 25 DPI. *N*=2 per group, each *N* includes 4 mice pooled. **b** tSNE plot of all immune cells analyzed in both mock- and WNV-infected animals, showing 9 clusters, colored by density clustering, and annotated by cell-type identity and number of cells in parentheses. **c** tSNE plots of all cells analyzed in mock (left panel)- and WNV (right panel)-infected mice, separated by treatment group, colored by density clustering. **d** Heatmap of single cells representing the mRNA levels of the top three well-known genes used for cellular identification of each cluster. **e** tSNE plot of all immune cells with mRNA of *Cxcr6* (left panel) and mRNA of *Cxcl16* (right panel). **f** Violin plots showing immune cells with *Cxcr6* mRNA (left panel) or *Cxcl16* mRNA (right panel) in clusters 0–5. Each dot represents a cell

of 4132 cells were obtained. After data normalization, cells were clustered into nine distinct clusters (Fig. 1b) using Seurat and visualized using t-distributed stochastic neighbor embedding (t-SNE).

Enriched genes for each cluster were determined by differential gene expression (DEG) analysis and used to identify cell clusters (Additional file 1: Table S1). As expected, not all clusters were present in high numbers in

Rosen *et al. Genome Medicine* (2022) 14:108

Page 7 of 20

both experimental groups (Fig. 1c, Additional file 1: Fig. S1a). Major CNS cell-type identities for each cluster were assigned by cross-referencing these genes with published gene expression datasets [31–35] (Fig. 1d, Additional file 1: Table S1). The annotated nine clusters included four microglia clusters, two T cell clusters, a macrophage cluster, an astrocyte cluster, and various other non-neuronal clusters. There were very low numbers of CD8^{+} and CD4^{+} T cells present in the mock-infected group. However, both CD8^{+} (cluster 2) and CD4^{+} (cluster 4) T cells were present in the WNV-infected group, consistent with previous data demonstrating very low levels of T cell entry into uninflamed CNS and T cell persistence in our model of WNV recovery [10, 39]. The homeostatic microglia cluster (cluster 0) was predominantly present in CNS cells from mock-infected mice, expressing known markers of microglial homeostasis, including *P2ry12* (purinergic receptor P2Y12), *Siglech* (sialic acid binding Ig-like lectin H), and *Csfr1* (colony-stimulating factor 1 receptor), while activated microglia clusters (clusters 1 and 3) was enlarged in the CNS cells from the WNV-infected mice, expressing *Cd74* (cluster of differentiation 74), histocompatibility 2 class II antigen genes,

Table 1 Top 25 defining genes of clusters 0, 1, and 3

Rank	Cluster 0	Cluster 1	Cluster 3	Cluster 7
1	*Fcrls*	*Cd74*	*Cd74*	*Enpp2*
2	*P2ry12*	*H2-Aa*	*Apoe*	*Mt3*
3	*Gpr34*	*H2-Ab1*	*Fth1*	*Clu*
4	*Hpgd*	*H2-Eb1*	*Ctss*	*Ppp1r1b*
5	*Fscn1*	*Ctss*	*Fcer1g*	*Ptgds*
6	*Cx3cr1*	*Lgals3bp*	*H2-Aa*	*Calml4*
7	*Sparc*	*H2-D1*	*Ftl1*	*Cryab*
8	*Cst3*	*C4b*	*Tyrobp*	*Rbp1*
9	*Olfml3*	*Fcgr4*	*Cxcl9*	*Cox8b*
10	*Siglech*	*Apoe*	*C1qb*	*Pcp4l1*
11	*P2ry13*	*Ly6e*	*Ctsb*	*Msx1*
12	*Pmp22*	*B2m*	*H2-Eb1*	*Igfbp2*
13	*Ecscr*	*Oasl2*	*Rps29*	*Fxyd1*
14	*Selplg*	*Ifi204*	*Eef1a1*	*Pcp4*
15	*Csf1r*	*Itm2b*	*Fau*	*Hemk1*
16	*Rnase4*	*Ccl12*	*Itm2b*	*Car2*
17	*Hexb*	*Ifitm3*	*H2-Ab1*	*Kl*
18	*Vsir*	*Ctsb*	*C1qa*	*Sostdc1*
19	*Serinc3*	*H2-Q6*	*B2m*	*Gsta4*
20	*Selenop*	*Ctsh*	*Psap*	*Prr32*
21	*Rhob*	*Fth1*	*Rplp1*	*Atp1b1*
22	*Tgfbr1*	*Cd72*	*H2-D1*	*Folr1*
23	*Golm1*	*Gm4951*	*Npc2*	*Kcnj13*
24	*Tmem119*	*Fcgr2b*	*Rpl21*	*Clic6*
25	*Slc2a5*	*Ctsc*	*Rps20*	*Crip2*

C4 (complement component 4), and *Apoe* (apolipoprotein E) (Table 1). Strikingly, the current dataset suggests that, even 10 days after WNV is cleared from the CNS, almost all microglia in the WNV-infected mice remain in an activated state. A fouth microglia cluster (cluster 7) was identified and categorized as an immediate early gene (IEG) microglia cluster (Table 1), which has shown to be an artifact of running the microglia through the 10x machine [40, 41].

scRNA-seq analysis identified two unique activated microglia clusters that persist in the forebrain of WNV-recovered mice

To investigate differences in the microglia clusters, we performed differential expression tests to compare microglia clusters 1 to 0 and 1 to 3. Genes important for MHC and antigen presentation, such as *Cd74*, *H2-Ab1*, and *H2-Eb1*, were found among the top 25 significantly upregulated genes in clusters 1 and 3, and homeostatic genes, such as *P2ry12*, *Cx3cr1*, *Fcrls*, *Siglech*, and *Hexb*, were found among the top 25 significantly upregulated genes in cluster 0 (Table 1). Thus, both clusters 3 and 1 downregulate homeostatic microglial genes, but cluster 1 appears to upregulate more genes responsible for antigen responses than cluster 3. GO biological processes pathway analysis between WNV cluster 1 and mock cluster 0, revealing upregulation in pathways involved in protein translation, antigen processing, and presentation of peptide antigen via MHC class I and class II in WNV cluster 1 vs mock cluster 0 (Additional file 1: Fig. S2a-b). To further investigate the effects of WNV infection on microglia, we examined the levels of known homeostatic markers between cluster 0 and clusters 1 and 3 from both mock and WNV-infected mice [11, 42, 43]. *P2ry12*, *Cx3cr1*, *Tmem119*, *Fcrls*, *Siglech*, *Gpr34*, and *Hexb* were all significantly decreased in clusters 1 and 3 compared to cluster 0 (Additional file 1: Fig. S2c-d). These data reveal a unique activated microglia signature that persists in the CNS of WNV-recovered animals that exhibit similarities to those observed in studies using murine models of neurodegenerative diseases [14, 43, 44].

Cxcl16 and Cxcr6 are uniquely upregulated by microglia and T cells in the forebrain of WNV-recovered animals

Although T cells are critical for viral clearance from the CNS, their persistence in the CNS after viral clearance contributes to persistent microglial activation [34, 45]. Chemokine signaling pathways are important for regulating the recruitment and migration of leukocytes into the CNS, and during acute WNV infection, infiltrating myeloid and T cells upregulate the expression of proinflammatory chemokine ligands and their receptors [46–49].

Rosen *et al. Genome Medicine* (2022) 14:108

Page 8 of 20

We identified *Cxcr6* as the only chemokine receptor in the top 25 DEGs within the CD8$^+$ T cell cluster in the WNV-recovered forebrain (Additional file 1: Table S2). *Cxcr6* was also highly upregulated in the CD4$^+$ T cell cluster in the WNV-recovered CNS (Fig. 1e, f). CXCR6 is the unique receptor for the transmembrane chemokine CXCL16 [17]. Consistent with this, *Cxcl16* was highly expressed in all of the myeloid cell populations in the WNV-recovered CNS (Fig. 1e, f). These data suggest that the CXCL16/CXCR6 chemokine signaling axis may be important for T cell recruitment or maintenance within the CNS during WNV infection.

CXCR6 is expressed by CD8$^+$ T cells that persist in the CNS after viral recovery

To validate and extend our scRNA-seq findings, we performed an analysis of mock- versus WNV-infected CXCR6-EGFP (green fluorescent protein) reporter mice at 25 DPI. Results revealed a significant increase in CXCR6$^+$ expressing cells in the forebrain of WNV-infected mice, which coincided with a significant increase in CXCR6$^+$CD3$^+$ co-localization via immunohistochemistry (Fig. 2a, b). In line with our scRNA-seq results, nearly 100% of the CXCR6$^+$ expressing cells were shown to be CD3$^+$, suggesting that T cells are the predominant source of CXCR6$^+$ in the WNV-recovered CNS (Fig. 2a, b). Flow cytometric analysis of CD45^{high} cells isolated from the forebrain of wild-type (WT) WNV-infected mice at 7 (peak encephalitis), 25 (early recovery), and 52 (late recovery) DPI indeed revealed a significant increase in percentages of CD4$^+$ and CD8$^+$ T cells expressing CXCR6 at 25 and 52 DPI compared to 7 DPI (Fig. 2c, Additional file 1: Fig. S3a,c). Further analysis revealed that approximately 100% of CD8$^+$CXCR6$^+$ in the CNS at 25 and 52 DPI express CD103, a marker for T$_R$M cells (Fig. 2d), consistent with our scRNA-seq findings (Additional file 1: Fig. S1d) and other studies linking CXCR6 to T$_R$M cell biology [27]. Furthermore, 100% of CD8$^+$IFNγ$^+$ cells were CXCR6$^+$ at 52 DPI (Additional file 1: Fig. S3f). MHC class I tetramer staining confirmed the specificity of these CD8$^+$ T cells to WNV NS4B, the immunodominant CD8 epitope in WNV-infected mice [50], and approximately 100% of the CD8$^+$NS4B$^+$T cells were CXCR6$^+$ in the CNS at 25 and 52 DPI (Fig. 2e). Additionally, approximately 100% of the CD8$^+$NS4B$^-$CD103$^+$ T cells were CXCR6$^+$ in the CNS at 25 and 52 DPI (Additional file 1: Fig. S3e). Within the meninges, about 20–30% of the CD8$^+$ T cells are CXCR6$^+$ at 25 and 52 DPI (Fig. 2h).

To determine whether CXCR6$^+$ upregulation on CD8$^+$ T cells occurs in the CNS or the periphery during WNV infection, we analyzed CXCR6 expression in the blood

and cervical lymph nodes (cLN). CD8$^+$ T cells in the blood upregulate CXCR6 at 7 DPI, with about 65% of CD8$^+$ T cells expressing CXCR6. However, during recovery at 25 and 52 DPI, only 8% of the CD8$^+$ T cells in the blood express CXCR6 (Fig. 2f). The percentage of CD8$^+$ CXCR6$^+$ T cells remained at about 5% in the cLN at 7 and 25 DPI and did decrease at 52 DPI, however not significantly (Fig. 2h). Of note, CD4$^+$ CXCR6$^+$ T cell percentages or numbers were not increased in the blood at any time point (Additional file 1: Fig. S3g). Taken altogether, these data suggest that high percentages of CD8$^+$ CXCR6$^+$ T cells are found within the blood as the cells traffic into the CNS via a route that includes the meninges and that they persist in the CNS throughout recovery.

Cxcl16 levels increase on IBA1$^+$ cells during acute infection and return to baseline levels during recovery

To validate scRNA-seq detection of *Cxcl16* mRNA expression within the WNV-recovered CNS, we performed in situ and immunohistochemical analysis of CNS tissues derived from mock- and WNV-infected mice at 7, 25, and 52 DPI. There was a significant increase in *Cxcl16* mRNA in WNV-infected tissue at 7 and 25 DPI compared to mock (Fig. 3a, b). Co-localization of *Cxcl16* within IBA1$^+$ cells detected increased levels in the cortex at 7 and 52 DPI, and the hippocampus at 7 and 25 DPI, compared to mock (Fig. 3c). Within the CNS, nearly 100% of the *Cxcl16* is co-localized with IBA1 at 7, 25, and 52 DPI, suggesting that myeloid cells are the predominant cellular source of *Cxcl16* (Fig. 3c, d). Notably, *Cxcl16* mRNA is found in the soma and processes of IBA1$^+$ cells at 7 DPI (Fig. 3a, white box inset), suggesting local translation of *Cxcl16* within cellular processes. These data indicate that *Cxcl16* is expressed by IBA1$^+$ cells within the CNS. To determine whether CXCL16 protein was being produced in the parenchyma of the CNS, we performed ELISA on cortical and hippocampal tissue, meninges, blood, and lymph nodes in mock- and WNV-infected mice at 7 and 25 DPI. CXCL16 levels were increased at 7 and 25 DPI in the cortex and 7 DPI in the hippocampus compared to mock. However, there was also a modest increase in CXCL16 in the cervical lymph nodes at 25 DPI (Fig. 3e), indicative of a peripheral source of CXCL16 during recovery that may be competing with CNS sources of CXCL16 to recruit CD8$^+$ T cells out of the CNS. To determine whether myeloid cells were interacting with CXCR6$^+$ T cells within the CNS, we examined CXCR6-EGFP reporter mice at 25 DPI and observed CD3$^+$CXCR6$^+$ T cells in close proximity to IBA1$^+$ cells (Fig. 3f). Together, these data suggest that CXCL16 from IBA1$^+$ myeloid cells may direct interactions with CD3$^+$ CXCR6$^+$ cells during CNS infection and recovery.
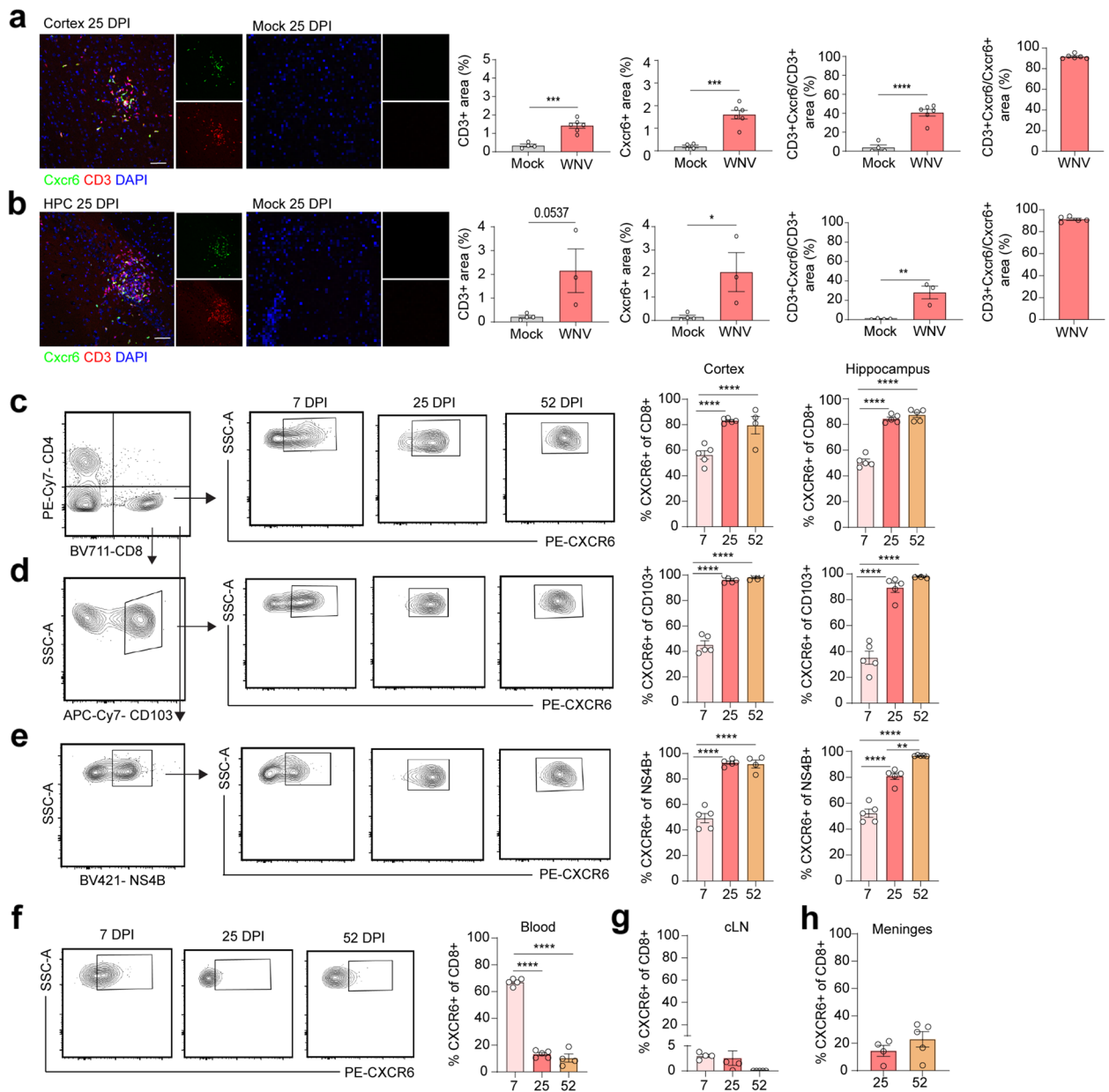
Fig. 2 CXCR6 is expressed by CD8^{+} T cells that persist in the CNS after viral recovery. **a**, **b** Immunohistological analysis for CXCR6 and CD3 in the cortex (**a**) and hippocampus (**b**) of mock- or WNV-infected mice at 25 DPI, presented as microscopy. The left graph shows the percenter CD3^{+} area, the middle left graph shows the percent CXCR6^{+} area, the right middle graph shows the CD3^{+}CXCR6^{+} area normalized to the total CD3^{+} area, indicative of co-localization, and the right graph shows the CD3^{+}CXCR6^{+} area normalized to the total CXCR6^{+} area. Scale bars, 50 μm. **c** Gating strategy and quantification of the percentage of CD8^{+} T cells that are CXCR6^{+} at 7, 25, and 52 DPI in the cortex (left graph) and hippocampus (right graph). Cells were gated on CD45^{high} (Additional file 1: Fig. S8a) before gating on CD4^{+} and CD8^{+} T cells (left panel). CD8^{+} T cells were then gated on CXCR6 (middle panels). **d** Gating strategy and quantification of the percentage of CD103^{+} cells that are CXCR6^{+} at 7, 25, and 52 DPI in the cortex and hippocampus. **e** Gating strategy and quantification of the percentage of NS4B^{+} cells that are CXCR6^{+} at 7, 25, and 52 DPI in the cortex and hippocampus. **f** Gating strategy and quantification of the percentage of CD8^{+} T cells that are CXCR6^{+} at 7, 25, and 52 DPI in the blood. Cells were gated on CD45^{high} before gating on CD4^{+} and CD8^{+} T cells. CD8^{+} T cells were then gated on CXCR6. **g** Quantification of the percentage of CD8^{+} T cells that are CXCR6^{+} at 7, 25, and 52 DPI in the cervical lymph nodes. **h** Quantification of the percentage of CD8^{+} T cells that are CXCR6^{+} at 25 and 52 DPI in the meninges. Gating for CXCR6 based off *Cxcr6*^{−/−} mice (Additional file 1: Fig. S8b, c). Data represent the mean±s.e.m. and were analyzed by unpaired Student's *t*-test. *$P<0.05$, **$P<0.005$, ***$P<0.001$, ****$P<0.0001$
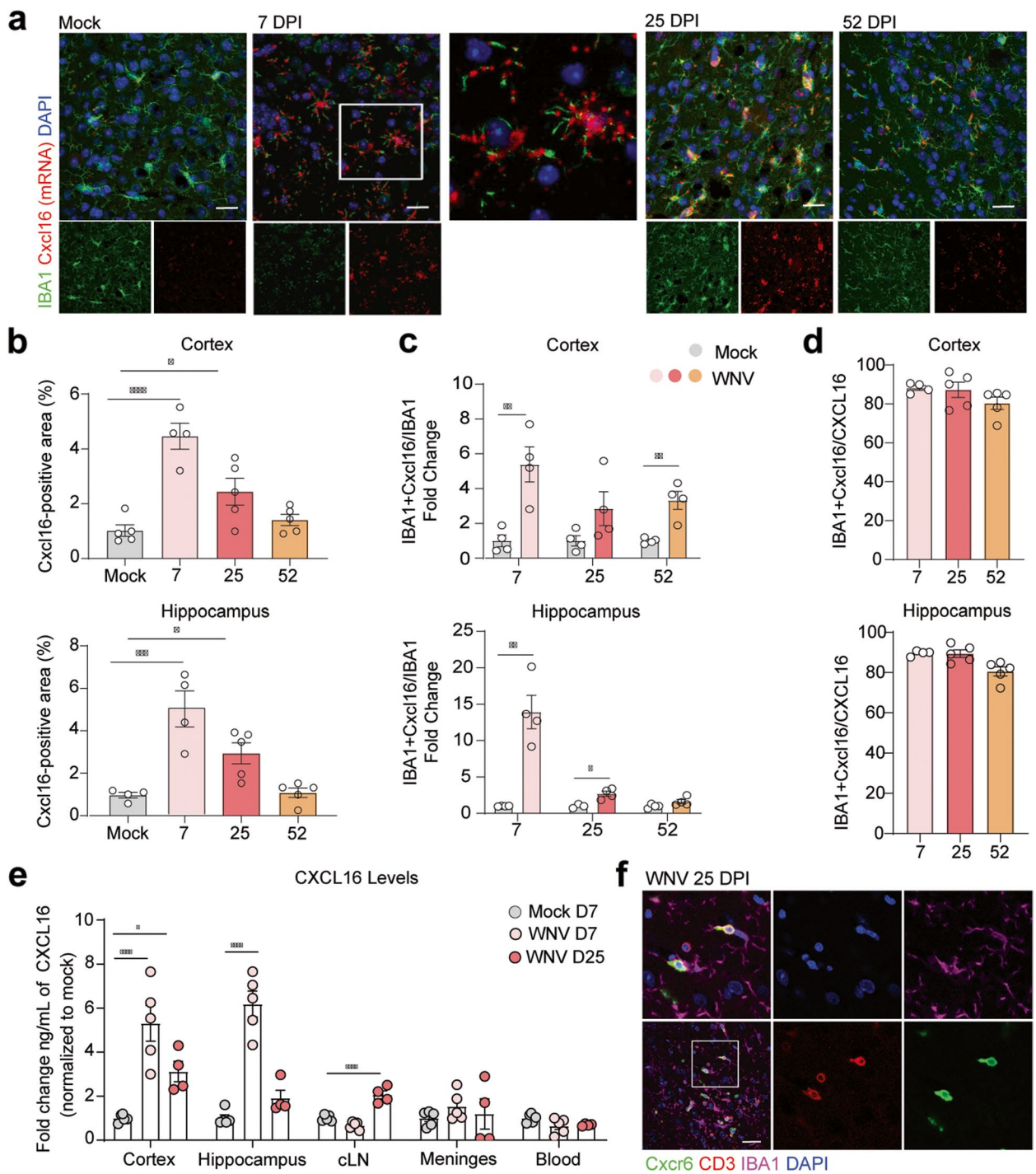
Fig. 3 CXCL16 levels increase on IBA1+ cells during acute infection and return to baseline levels during recovery. **a** Representative microscopy images of RNA in situ/immunohistochemistry (ISH/IHC) for *Cxcl16* and IBA1 in the cortex of mock- or WNV-infected mice at 7, 25, ad 52 DPI. The middle panel is the inset of the white box in 7 DPI. **b–d** Quantification of the ISH/IHC for *Cxcl16*+ area (**b**); IBA1+*Cxcl16*+ area normalized to the total IBA1+ area, represented as fold change over mock (**c**); or IBA1+*Cxcl16*+ area normalized to the total *Cxcl16*+ area (**d**) in the cortex or hippocampus of mock- or WNV-infected mice at 7, 25, and 52 DPI. **e** ELISA for CXCL16 in the cortex, hippocampus, cervical lymph nodes, meninges, and blood at 7 and 25 DPI. **f** Representative immunostaining of the cortex for CXCR6-GFP, CD3, IBA1, and DAPI. Scale bars, 50 μm. Data represent the mean±s.e.m. and were analyzed by one-way ANOVA or unpaired Student's *t*-test. *$P<0.05$, **$P<0.005$, ***$P<0.001$, ****$P<0.0001$
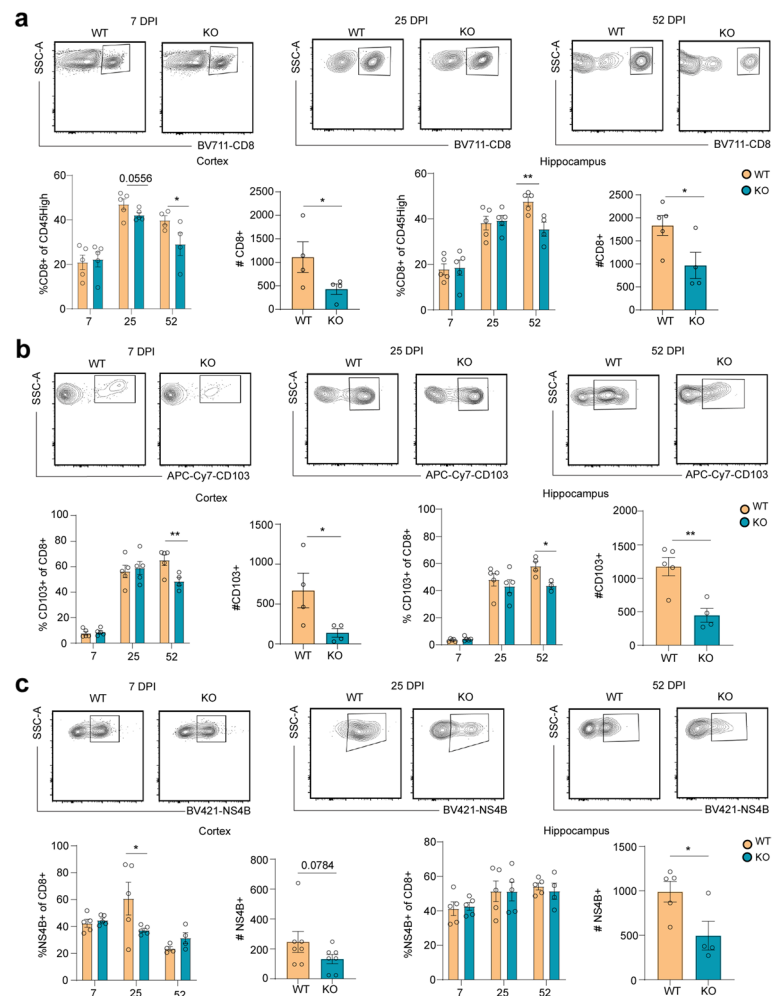
Fig. 4 *Cxcr6⁻/⁻* animals have decreased maintenance of CD8⁺ T cells in the post-infectious CNS. **a** Representative gating strategy and quantification of the percentage of CD8⁺ T cells within the cortex and hippocampus at 7, 25, and 52 DPI (left graph), followed by total CD8⁺ cell numbers at 52 DPI in WT versus *Cxcr6⁻/⁻* mice (right graph). **b** Representative gating strategy and quantification of the percentage of CD103⁺ cells within the cortex and hippocampus at 7, 25, and 52 DPI, followed by total CD103⁺ cell numbers at 52 DPI, in WT versus *Cxcr6⁻/⁻* mice. **c** Representative gating strategy and quantification of the percentage of NS4B⁺ cells within the cortex and hippocampus at 7, 25, and 52 DPI, followed by total NS4B⁺ cell numbers at 52 DPI in WT versus *Cxcr6⁻/⁻* mice. Cells were gated according to the gating strategy in Additional file 1: Fig. S8. Data represent the mean±s.e.m. and were analyzed by unpaired Student's *t*-test at 7, 25, and 52 DPI. *$P<0.05$, **$P<0.005$

CXCR6 is not required for CNS virologic control during acute WNV infection

To determine whether CXCR6 contributes to antiviral T cell responses within the CNS during acute infection, we examined immune cell infiltration and viral clearance in WT and *Cxcr6⁻/⁻* mice. First, we confirmed the deletion of CXCR6 on both CD8⁺ and CD4⁺ T cells in the forebrain of *Cxcr6⁻/⁻* mice (Additional file 1: Fig. S4e, f). Analysis of CD45^high cells at 7 DPI revealed no differences in frequency or number of CD4⁺, CD8⁺, CD103⁺, or NS4B⁺ T cells in the forebrain between WT and *Cxcr6⁻/⁻* mice (Fig. 4a, b, c. Additional file 1: Fig. S4h, i). There were also no significant differences in

the percentages of CD8⁺ or CD4⁺ T cells in the blood between WT and *Cxcr6⁻/⁻* mice at 7 DPI (Additional file 1: Fig. S4l). Furthermore, WNV infection of WT and *Cxcr6⁻/⁻* mice did not reveal significant differences in survival, weight loss, acute levels, or clearance of viral loads in the CNS (Additional file 1: Fig. S4a, b, c, d). These data suggest that CXCR6 is not required for the trafficking and antiviral functions of T cells in the CNS.

CXCR6 is required for the maintenance of CD8⁺ T_RM cells in the forebrain after recovery from WNV

Given the high expression of CXCR6 on T cells within the CNS after viral recovery, we hypothesized that CXCR6

may play an important role in the maintenance of CD4+ and/or CD8+ T cells in the CNS. To test this hypothesis, we performed phenotypic analyses of infiltrating T cells in the CNS and peripheral tissue from mock- and WNV-infected wild-type (WT) and *Cxcr6*−/− mice at 25 and 52 DPI. At 25 DPI, there was a trend towards a decrease in the percentage of CD8+ T cells and a significant decrease in the percentage of CD8+NS4B+ T cells in the cortex in *Cxcr6*−/− compared with WT animals (Fig. 4a, d). However, there were no differences in the percentage of CD103+ or numbers of CD8+, CD103+, or NS4B+ in the cortex at 25 DPI (Fig. 4a, b, c, Additional file 1: Fig. S5b). Similarly, there were no significant differences in percentages or numbers of CD8+, CD103+, or NS4B+ in the hippocampus at 25 DPI (Fig. 4a, b, c, Additional file 1: Fig. S5b). In contrast, at 52 DPI, there were significant decreases in both percentages and numbers of CD8+ and CD8+CD103+ cells in both CNS regions of WNV-recovered *Cxcr6*−/− mice compared with WT mice (Fig. 4a, b). Of note, the percentages of CD8+NS4B+ cells were not significantly different at 52 DPI in either brain region, nor were there differences in percentages of CD103+CD8+ that were NS4B+ at 7, 25, or 52 DPI, suggesting that CXCR6 is not required for the maintenance of virus-specific CD8+ T cells (Fig. 4c, Additional file 1: Fig. S4g). However, the numbers of CD8+NS4B+ T cells were significantly lower in both the hippocampi and cortices of *Cxcr6*−/− mice compared to WT mice at 52 DPI, which is likely a result of a decrease in total CD8+ T cells in the forebrain (Fig. 4c). We also did not see any significant differences in CD4+ T cell numbers in the CNS at 25 or 52 DPI between WT and *Cxcr6*−/− mice (Additional file 1: Fig. S4h, i). These data suggest that CXCR6 is necessary for the persistence of CD8+ T cells in the CNS after recovery from viral infection.

Terminal deoxynucleotidyl transferase dUTP nick end labeling (TUNEL) and CD3+ immunodetection within the hippocampi and WNV-recovered WT and *Cxcr6*−/− mice at 52 DPI did not reveal any differences between the genotypes (Additional file 1: Fig. S6a). This suggests that increased rates of apoptosis are not responsible for the loss of T$_R$M cells in the CNS of *Cxcr6*−/− mice. Similarly, analysis of hippocampi from WT and *Cxcr6*−/− CD8+ T cell at 35 DPI for expression of CCR7 and CD62L, a chemokine receptor and selectin, respectively, with known roles in facilitating the homing of memory CD8+ T cells back to lymph nodes [51, 52], did not reveal any significant differences between the genotypes (Additional file 1: Fig. S6b). For these studies, day 35 was chosen as a midpoint between 25 to 52 DPI, the latter of which was when we detected significantly decreased percentages and numbers of CD8+ T cells in the forebrain of *Cxcr6*−/− mice. Further analysis of meningeal T cells at

25 and 52 DPI did not reveal any significant differences in the percentage of CD8+, NS4B+, CD103+, or CD4+ cells between WT and *Cxcr6*−/− mice (Additional file 1: Fig. S4j). Analysis of the blood and cLN also did not reveal any significant differences in the percentages or numbers of CD8+CXCR6+ or CD4+CXCR6+ cells between WT and *Cxcr6*−/− mice at 25 or 52 DPI (Additional file 1: Fig. S4k, i). Together, these results suggest that the loss of CD8+ T cells from the CNS of *Cxcr6*−/− mice is not attributable to substantial differences in apoptosis, egress to the lymph node, or accumulation in the meninges.

CXCR6 signaling contributes to persistent microglial activation and impaired synapse recovery in the hippocampi of WNV-infected animals

We previously showed that CD8+ T$_R$M cell-derived IFNγ signaling is required for microglial activation and astrocyte expression of interleukin (IL)-1β within the hippocampus of WNV-recovered mice [10]. Given the significant decrease in CD8+CD103+ cells in the hippocampi of WNV-recovered *Cxcr6*−/− mice, we hypothesized that CXCR6-deficient mice would exhibit attenuation of these responses during recovery from WNV infection. Consistent with prior studies demonstrating that IFNγ signaling is required for the generation of IL-1β producing astrocytes [53], we detected increased IL-1β expression by GFAP+ astrocytes in the hippocampi of WNV-infected WT mice at 52 and 25 DPI compared with mock-infected animals (Fig. 5a, Additional file 1: Fig. S7a). Although astrocyte expression of IL-1β was also elevated in *Cxcr6*−/− mice at 25 DPI compared with mock-infected animals, it was significantly lower than that observed in WNV-infected WT mice at 52 DPI (Additional file 1: Fig. S7a, Fig. 5a). There were no significant differences in GFAP expression between any of the groups at 52 DPI (Fig. 5a). Similarly, while WNV infection led to increased IBA1+ expression within the hippocampus of WT and *Cxcr6*−/− mice at 25 DPI compared to mock (Additional file 1: Fig. S7a), at 52 DPI *Cxcr6*−/− mice exhibited significantly less IBA1+ expression the hippocampus compared to similarly infected WT mice (Fig. 5b). These data are consistent with the findings that WNV-specific CD8+ T cells are found in similar numbers in the CNS of WT and *Cxcr6*−/− mice at 25 DPI, but are significantly lower in *Cxcr6*−/− mice at 52 DPI (Fig. 4a). Notably, while WNV-recovered *Cxcr6*−/− mice exhibited significantly higher IBA1+ expression compared to mock-infected controls, they exhibited significantly lower IBA1+ expression than WT controls. Together, these data suggest that CD8+CXCR6+ T cells in the hippocampus play a role in maintaining phagocytic microglia and astrocyte expression of IL-1β within the hippocampus of WNV-infected animals during recovery.
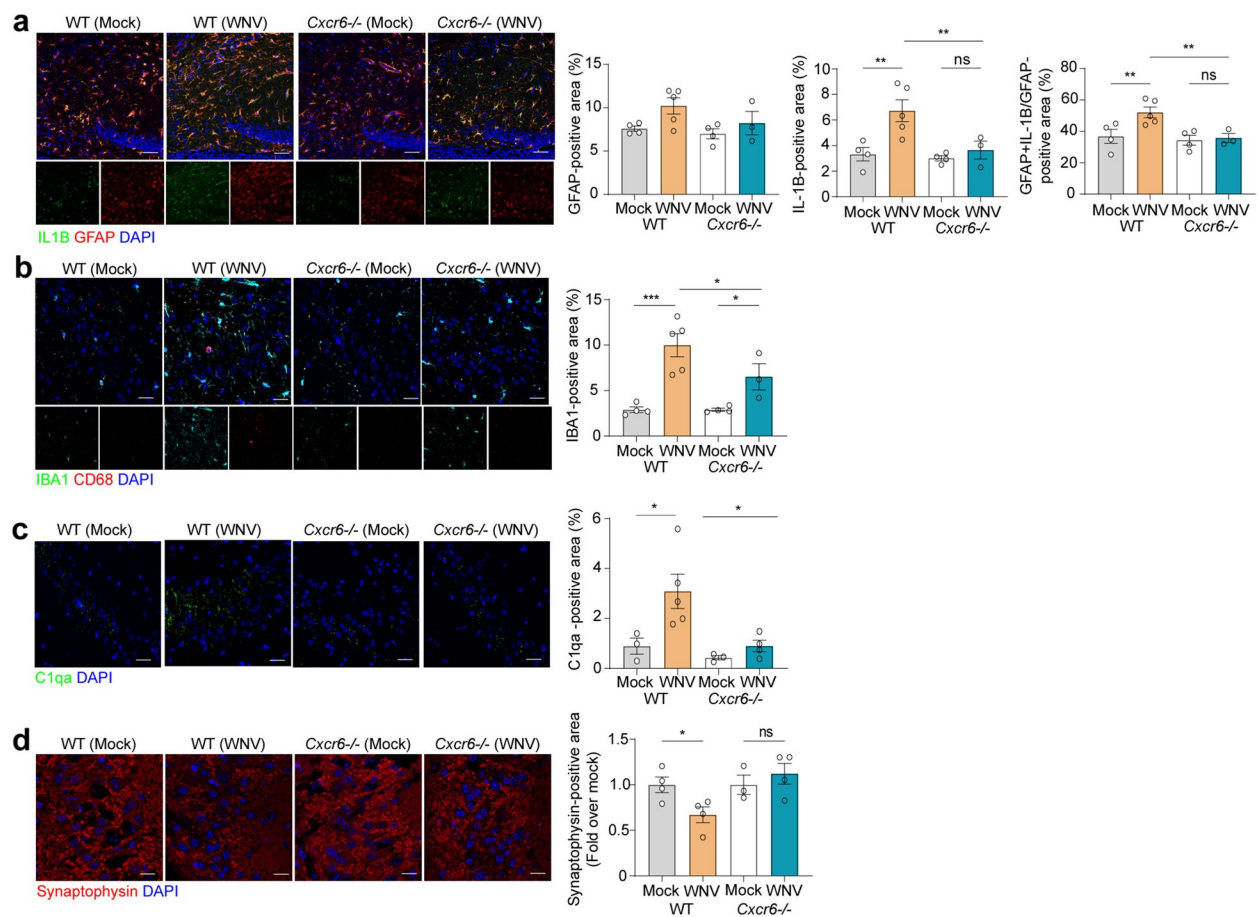
Rosen *et al. Genome Medicine*   (2022) 14:108

Page 13 of 20

Fig. 5 CXCR6 signaling potentiates gliosis in the recovered hippocampi of WNV-infected animals, contributing to synaptic elimination. **a** Representative immunostaining and quantification of IL-1β (green), GFAP (red), and DAPI (blue) in the CA3 region of the hippocampus of mock or WNV-infected WT or *Cxcr6*$^{-/-}$ mice at 52 DPI. GFAP quantified by percent positive area, IL-1β quantified by percent positive area, followed by quantification of GFAP$^+$IL-1β$^+$ area, normalized to the total GFAP$^+$ area. **b** Representative immunostaining and quantification of IBA1 (green), CD68 (red), and DAPI (blue) in the hippocampus of mock- or WNV-infected WT or *Cxcr6*$^{-/-}$ animals at 52 DPI. IBA1$^+$ quantified as percent positive area. **c** Representative immunostaining and quantification of C1qa in the hippocampus of mock- or WNV-infected WT or *Cxcr6*$^{-/-}$ animals at 52 DPI showing staining for C1qa (green) and DAPI (blue). C1qa quantified as percent positive area. **d** Representative immunostaining and quantification of synapses in the CA3 region of the hippocampus in mock- or WNV-infected WT or *Cxcr6*$^{-/-}$ animals at 52 DPI showing staining for synaptophysin (red) and DAPI (blue). Synaptophysin quantified by percent positive area. Scale bars, 50 μm (**a**–**c**) or 20 μm (**d**). Data represent the mean±s.e.m. and were analyzed by two-way ANOVA and corrected for multiple comparisons. *$P<0.05$, **$P<0.005$, ***$P<0.001$

Given the significant decrease in IBA1$^+$ cells within the hippocampi of WNV-recovered *Cxcr6*$^{-/-}$ mice compared to WT animals, we wondered whether CXCR6-deficient mice would also exhibit decreased complement and microglial-mediated synapse elimination, which was especially profound in the CA3 region of hippocampi in WT animals [9]. At 25 DPI, both WNV-recovered WT and *Cxcr6*$^{-/-}$ mice exhibited loss of presynaptic terminals, as assessed by detection of synaptophysin (Additional file 1: Fig. S7c). However, at 52 DPI, only WT mice continued to exhibit decreased presynaptic terminals compared to mock (Fig. 5d). Additionally, at 52 DPI, WNV-recovered *Cxcr6*$^{-/-}$ mice

exhibited similar levels of synaptophysin as mock-infected *Cxcr6*$^{-/-}$ mice, and immunohistochemical examination of C1QA protein within the CA3 region of the hippocampus in mock- versus WNV-recovered mice revealed no differences in *Cxcr6*$^{-/-}$ mice, but a significant increase in WT WNV-recovered mice (Fig. 5c). Together, these data suggest that decreases in C1QA, microglial activation, and astrocyte IL-1β expression prevented ongoing synapse elimination in *Cxcr6*$^{-/-}$ mice (Fig. 5d, Additional file 1: Fig. S7c). These studies demonstrate a critical role for CXCR6 in promoting injury to the hippocampal synaptic circuit through the regulation of CD8$^+$ T cell number

Rosen *et al. Genome Medicine*   (2022) 14:108

Page 14 of 20

and microglial activation within the WNV-recovered hippocampus.

CD8⁺CXCR6⁺ T cells maintain T_RM cells and synapse elimination in the forebrain after recovery from WNV infection

To confirm that CXCR6 specifically on CD8⁺ T cells is required for maintenance of $T_R M$ cells, microglial activation, and synapse elimination in the hippocampus after WNV recovery, naïve CD8⁺ T cells were isolated from the spleens of WT or $Cxcr6^{-/-}$ mice and adoptively transferred (AT) into $Cd8^{-/-}$ mice. $Cd8^{-/-}$ mice were infected 24 h after AT, followed by harvesting of CD8⁺ T cells from the CNS at 52 DPI (Fig. 6a). Phenotypic analysis revealed that recipients of CD8⁺ T cells derived from $Cxcr6^{-/-}$ mice exhibited significantly lower percentages of CD8⁺NS4B⁺ and CD8⁺CD103⁺ cells in the forebrain than those that received WT CD8⁺ T cells (Fig. 6b, c). Upon examination of the CD8⁺ T cells that did persist within the CNS of mice that received WT CD8⁺ T cells, CXCR6 was expressed on approximately 100% (Fig. 6b), confirming that CXCR6 is essential for the generation of $T_R M$ cells. Importantly, mice that received CD8⁺ T cells from $Cxcr6^{-/-}$ mice also exhibited significantly lower immunodetection of IBA1⁺ percent area compared to mice that received WT CD8⁺ T cells (Fig. 6d). Finally, mice that received $Cxcr6^{-/-}$ CD8⁺ T cells exhibited significantly higher levels of synaptophysin than those that received WT CD8⁺ T cells (Fig 6e). Together, these data suggest a cell-intrinsic role for CXCR6 in promoting CD8⁺ $T_R M$ cell maintenance in the CNS after viral encephalitis, contributing to persistent microglial activation and synaptic elimination.

CXCL16 neutralization leads to decreased frequency of T_RM cells in the WNV-recovered forebrain
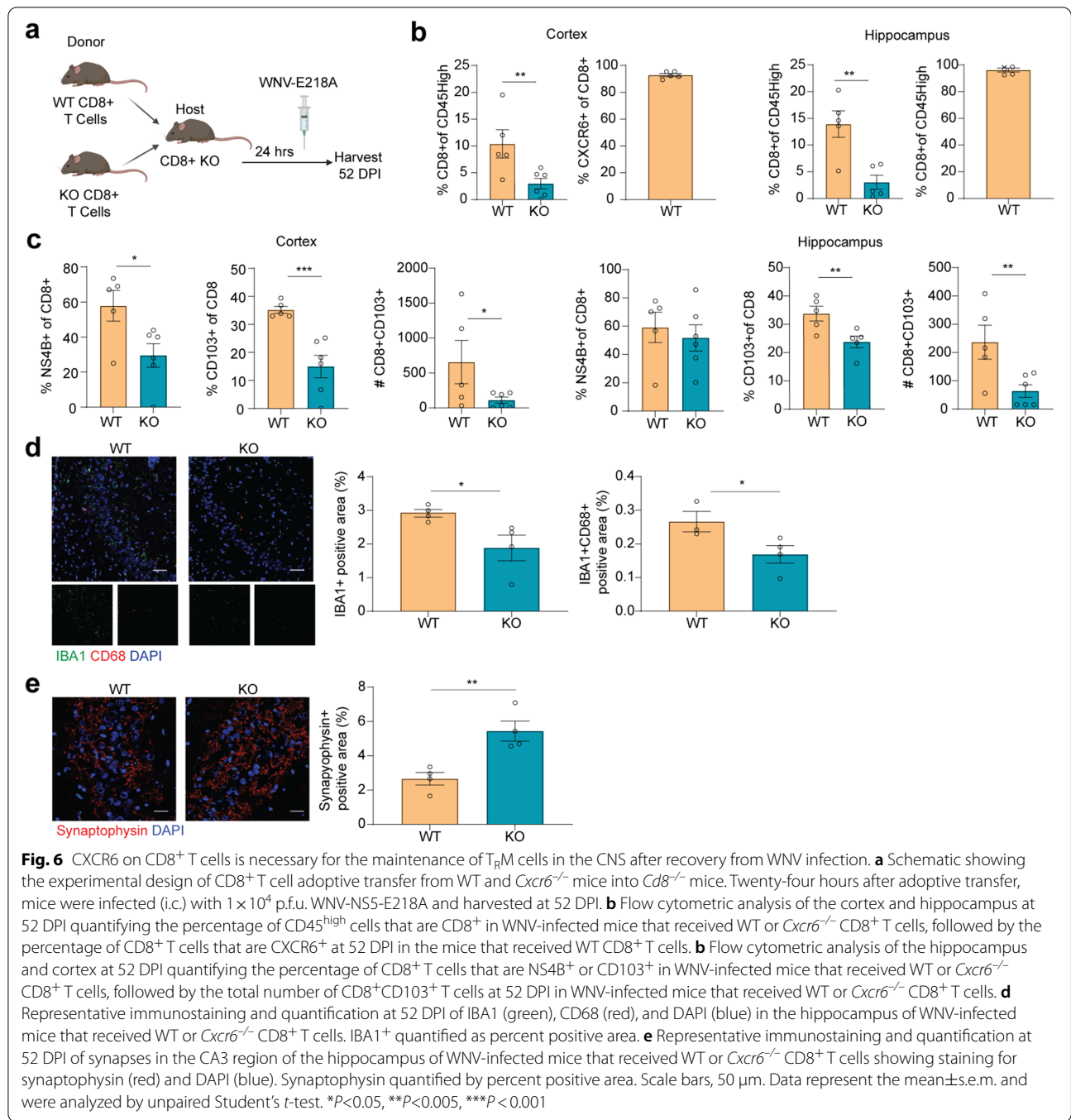
Given our findings that CXCR6 signaling generates and maintains CD8⁺CD103⁺ T cells in the forebrains of WNV-recovered and that this is required for neuropathology that contributes to cognitive dysfunction, we hypothesized that exogenous neutralization of CXCL16 might prevent maintenance of CD8⁺ $T_R M$ cells. To test this hypothesis, we intravenously administered CXCL16 neutralizing monoclonal antibody (NmAb) versus PBS (Additional file 1: Fig. S8) or isotype (Fig. 7) controls to WT WNV-infected mice at 7, 8, 9, and 10 DPI (Fig. 7a). These time points were chosen based on published data indicating that permeability of the blood-brain barrier peaks at 9 DPI in our model of WNV recovery [53]. Forebrain CD8⁺CD103⁺ T cells remained significantly lower in the anti-CXCL16 NmAb-treated group at 25 DPI (Additional file 1: Fig. S8); however, the differences were more robust at 15 DPI (Additional file 1: Fig. 8, Fig. 7).

This is consistent with previous studies demonstrating differentiating $T_R M$ cells responding to acute infections robustly express CD103 at this timepoint [54]. As expected, there were no significant decreases in the percentages of total CD8⁺ T cells in the forebrain of the anti-CXCL16 NmAb-treated group. These data indicate that antibody-based neutralization of CXCL16 limits the generation of forebrain CD8⁺CD103⁺ T cells and suggests CXCL16 might be a therapeutic target.
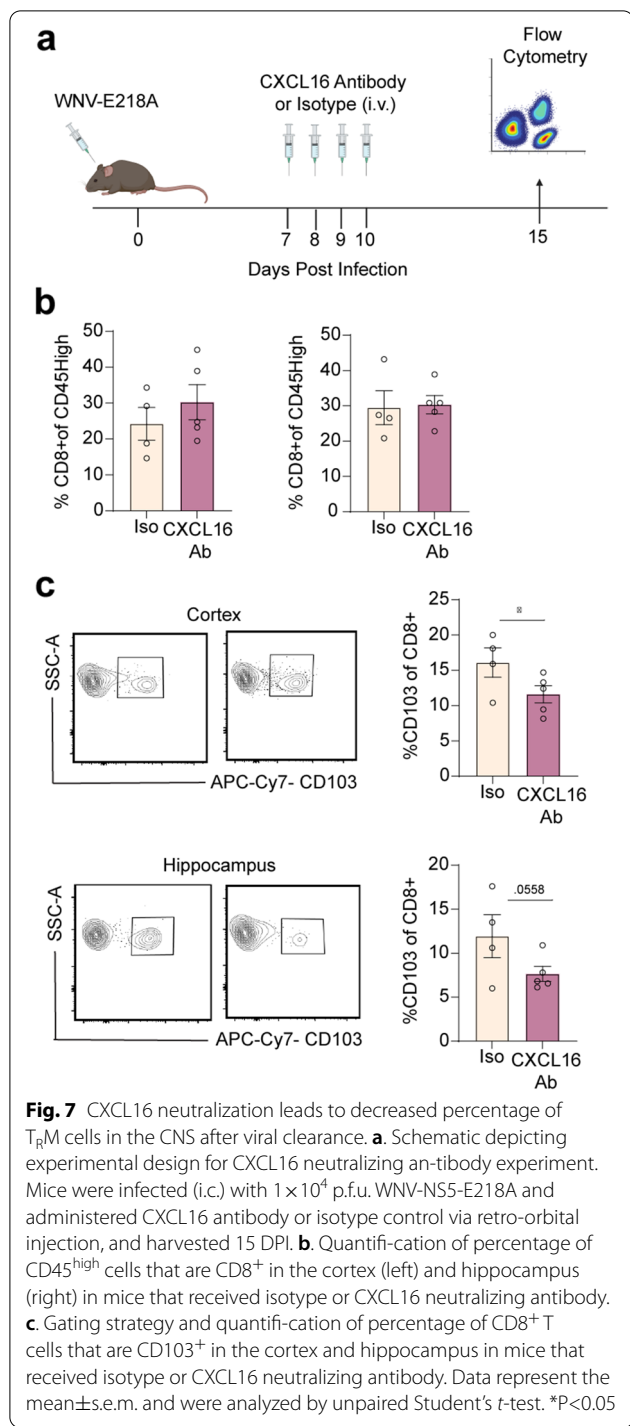
Discussion

During viral encephalitis, infection of neural cells leads to the activation of resident glial cells, such as microglia and astrocytes, induction of cytokines and chemokines, and leukocyte invasion into the CNS [8]. The extent to which acute infection and inflammation contribute to disease pathology during recovery is complex, involving the coordination of multiple cell types and their subpopulations, each with distinct functions [55, 56]. Prior to the advent of scRNA-seq, which enables profiling of single cells without prior gene knowledge and clustering based on transcriptional signatures, unbiased investigation of cells that persist within the CNS after recovery from viral encephalitis, and their functional consequences, has been difficult. Here, we identified eleven cell clusters present in the WNV-recovered forebrain, including four microglia clusters, two T cell clusters, a macrophage cluster, an astrocyte cluster, and various other nonneuronal clusters. It is important to note that relatively fragile cells, such as neurons and oligodendrocytes, are often reduced or lost during processing for scRNA-seq [57]. Thus, the 11 cell clusters identified here are not a complete representation of all of the cell types present in the WNV-recovered forebrain. Of the myeloid clusters identified, we detected unique activated microglia clusters that express the chemokine *Cxcl16* and found that all persisting CD8⁺ T cells and many CD4⁺ T cells express CXCL16's only receptor, CXCR6. Using mice with global deletion of *Cxcr6* or intravenous administration of CXCL16 neutralizing antibodies, we showed that CXCL16/CXCR6 differentiate and maintain forebrain $T_R M$ cells and are required for microglial and astrocyte activation and ongoing synapse elimination in virally recovered animals

Microglia are CNS-resident mononuclear phagocytic cells that are important for both immune protection via the expression of pattern recognition receptors (PRRs) and neuronal function by regulating homeostasis and synaptic remodeling [58]. ScRNA-seq analyses of microglia have previously demonstrated their heterogeneity and that they adapt their gene expression profiles during development, homeostasis, and perturbations [11, 59]. Microglia in the uninflamed brain exhibit a homeostatic

Fig. 6 CXCR6 on CD8$^+$ T cells is necessary for the maintenance of T$_R$M cells in the CNS after recovery from WNV infection. **a** Schematic showing the experimental design of CD8$^+$ T cell adoptive transfer from WT and *Cxcr6$^{-/-}$* mice into *Cd8$^{-/-}$* mice. Twenty-four hours after adoptive transfer, mice were infected (i.c.) with 1×10^4 p.f.u. WNV-NS5-E218A and harvested at 52 DPI. **b** Flow cytometric analysis of the cortex and hippocampus at 52 DPI quantifying the percentage of CD45^{high} cells that are CD8$^+$ in WNV-infected mice that received WT or *Cxcr6$^{-/-}$* CD8$^+$ T cells, followed by the percentage of CD8$^+$ T cells that are CXCR6$^+$ at 52 DPI in the mice that received WT CD8$^+$ T cells. **b** Flow cytometric analysis of the hippocampus and cortex at 52 DPI quantifying the percentage of CD8$^+$ T cells that are NS4B$^+$ or CD103$^+$ in WNV-infected mice that received WT or *Cxcr6$^{-/-}$* CD8$^+$ T cells, followed by the total number of CD8$^+$CD103$^+$ T cells at 52 DPI in WNV-infected mice that received WT or *Cxcr6$^{-/-}$* CD8$^+$ T cells. **d** Representative immunostaining and quantification at 52 DPI of IBA1 (green), CD68 (red), and DAPI (blue) in the hippocampus of WNV-infected mice that received WT or *Cxcr6$^{-/-}$* CD8$^+$ T cells. IBA1$^+$ quantified as percent positive area. **e** Representative immunostaining and quantification at 52 DPI of synapses in the CA3 region of the hippocampus of WNV-infected mice that received WT or *Cxcr6$^{-/-}$* CD8$^+$ T cells showing staining for synaptophysin (red) and DAPI (blue). Synaptophysin quantified by percent positive area. Scale bars, 50 μm. Data represent the mean±s.e.m. and were analyzed by unpaired Student's *t*-test. *$P<0.05$, **$P<0.005$, ***$P<0.001$

genetic signature, expressing mRNAs for *P2ry12*, *Cx3cr1*, *Temem119*, *Siglech*, *Hexb*, and *Fcrls*, which are all downregulated during aging and in neurodegenerative diseases associated with cognitive disruption [60, 61]. We see that recovery from CNS infection with WNV, which may induce spatial learning defects, is also associated with downregulation of these homeostatic microglial gene signatures. Consistent with this, activated microglia cluster 1 instead upregulates genes involved in antiviral defense, peptide metabolic processes, antigen processing and presentation, and protein synthesis, such as *Cd74*, *Ifitm3*, *H2-Ab1*, *B2m*, *Ctss*, and *Apoe*, while cluster 3 additionally expressed high levels of *Tyrobp*, *Fcer1g*, and *Cxcl9*. Notably, microglial expression of these genes has been implicated in aging or neurodegenerative disorders such as Alzheimer's and Parkinson's diseases and

Rosen *et al. Genome Medicine*   (2022) 14:108

Page 16 of 20

Fig. 7 CXCL16 neutralization leads to decreased percentage of T_RM cells in the CNS after viral clearance. **a**. Schematic depicting experimental design for CXCL16 neutralizing an-tibody experiment. Mice were infected (i.c.) with 1×10^4 p.f.u. WNV-NS5-E218A and administered CXCL16 antibody or isotype control via retro-orbital injection, and harvested 15 DPI. **b**. Quantifi-cation of percentage of $CD45^{high}$ cells that are $CD8^+$ in the cortex (left) and hippocampus (right) in mice that received isotype or CXCL16 neutralizing antibody. **c**. Gating strategy and quantifi-cation of percentage of $CD8^+$ T cells that are $CD103^+$ in the cortex and hippocampus in mice that received isotype or CXCL16 neutralizing antibody. Data represent the mean±s.e.m. and were analyzed by unpaired Student's *t*-test. *P<0.05

for CXCL16, which is upregulated in activated microglia clusters and in macrophages that persist in the forebrain of WNV-recovered mice. CXCL16 is expressed on the surface of APCs, such as monocyte-derived and conventional dendritic cells, promoting immune cell chemotaxis [18, 64]. Past studies have shown that CXCL16 is important for the localization of infiltrating $CD8^+$ T cells within inflamed tissues [27]. Using an established model of WNND recovery, we detected the highest levels of CXCL16 at 7 DPI, when the percentage of $CD8^+CXCR6^+$ T cells are lowest in the CNS. During recovery, at 52 DPI, when almost 100% of the $CD8^+$ T cells express CXCR6, the levels of CXCL16 return to mock-infected levels. Furthermore, we see opposite trends of $CD8^+CXCR6^+$ levels in the blood and CNS, with the highest levels of $CD8^+CXCR6^+$ T cells in the blood at 7 DPI, when $CD8^+CXCR6^+$ T cells in the forebrain are lowest, and the lowest levels of $CD8^+CXCR6^+$ T cells in the blood at 52 DPI, when $CD8^+CXCR6^+$ T cells in the forebrain are highest. Therefore, either only the infiltrated $CXCR6^+$ $CD8^+$ T cells from the blood persist within the CNS of WNV-recovered animals or CXCR6 is upregulated upon CNS infiltration of $CD8^+$ T cells. If the latter occurred, it would likely be due to meningeal signals [30]. Our data suggests that the former is more likely because total $CD8^+$ T cell numbers decrease in the cortex and hippocampus as CXCL16 levels wane.

$CD8^+$ T cells are key players in virologic control and may persist as T_RM cells in the CNS for years after recovery from neurotropic viral infections [65] via unknown mechanisms. Published studies have demonstrated pathogen-specific T_RM cells exhibit increased expression of CXCR6, which maintains them in the liver following malaria infection, and in the lung after influenza infection [26, 27]. Similarly, In the skin, CXCR6 expression by $CD8^+$ T cells is required for optimal formation of T_RM populations after epicutaneous infection with HSV-1 KOS [66]. Conversely, CXCR6 deficiency in the setting of infection with *Mycobacterium tuberculosis* (mTB) results in decreased bacterial burden without reduction in the number of T_RM cells in the lungs [67]. These studies suggest that CXCR6 expression on $CD8^+$ T cells has a distinct role dependent upon the type of infection. After infection with WNV, $Cxcr6^{-/-}$ mice exhibit a similar frequency of virus-specific $CD8^+$ T cells as WT mice in the forebrain, indicating no role for CXCR6 in T cell recruitment at peak CNS viral loads. In addition, $Cxcr6^{-/-}$ mice did not demonstrate any differences in weight loss, survival, or viral titers, suggesting that CXCR6 is not necessary for an effective immune response after WNV encephalitis, or trafficking of $CD8^+$ T cells into the CNS parenchyma. By 52 DPI, however, $Cxcr6^{-/-}$ mice have significantly less $CD8^+CD103^+$ T cells compared to WT.

multiple sclerosis [14, 43, 44, 62, 63]. These data suggest viral encephalitis may be a trigger for progressive neurodegenerative diseases.

Upon investigation of the top 25 genes in the T cell clusters, we identified *Cxcr6* as one of the top DEGs in the $CD8^+$ T cell cluster. CXCR6 is the unique receptor

While the scRNA-seq data demonstrate high expression of CXCR6 on CD4$^+$ T cells in the WNV-recovered fore-brain, similar analyses revealed no differences in levels of CD4$^+$ T cells between WNV-infected WT and *Cxcr6*$^{-/-}$ mice at any DPI. These data suggest CXCR6 expression by CD8$^+$ T cells is required to maintain and, possibly, differentiate T$_R$M cells within the CNS. Indeed, adoptive transfer of CXCR6-deficient CD8$^+$ T cells into *Cd8*$^{-/-}$ mice, followed by WNV infection, led to essentially no CD8$^+$CD103$^+$ T cells in the forebrain at 52 DPI. On the contrary, *Cd8*$^{-/-}$ mice that received WT CD8$^+$ T cells exhibited high levels of CD8$^+$CD103$^+$ T cells at 52 DPI, 100% of which were CXCR6$^+$. Thus, CXCR6 expression on CD8$^+$ T cells is necessary for their maintenance as T$_R$M cells within the CNS after WNV encephalitis.

We previously showed that CD8$^+$ T cell-derived IFNγ signaling in microglia underlies spatial learning and cognitive deficits during recovery from WNV, and mice deficient in CD8$^+$ T cells do not exhibit synapse loss during WNV infection [10]. Here, we found that 100% of all CD8$^+$IFNγ$^+$ T cells in WNV-recovered animals WT mice are also CXCR6$^+$. Given that IFNγ produced from CD8$^+$ T cells is responsible for persistent microglial activation, it is not surprising that *Cxcr6*$^{-/-}$ mice, which do not maintain CD8$^+$ T cells, have decreased microglial activation at 52 DPI. We have also previously shown that WNV-recovered mice exhibit increased astrocyte expression of IL-1β within the hippocampus [53]. In this study, we show that *Cxcr6*$^{-/-}$ mice have attenuated astrocytic production of IL-1β in the hippocampus at 52 DPI compared to WT WNV-infected mice, suggesting T$_R$M cells are important for astrocyte activation. While it has been shown that CXCL16 can act on astrocytes to promote hippocampal neuroprotection against excitotoxic damage [22], our data suggests that this effect is likely due to lack of microglial activation, as, in previous studies, we found that this associated with lack of IL-1β expression by astrocytes [10].

Finally, as CD8$^+$ T cells are necessary for viral clearance, but their persistence in the CNS can lead to chronic microglial activation and long-term cognitive sequelae [10, 33, 68], therapies that restrict T$_R$M generation without disrupting CD8$^+$ T cell antiviral functions may be valuable. To test this, we administered neutralizing anti-murine CXCL16 antibodies (Ab) during peak infection. We found anti-CXCL16 Ab, but not administration of isotype control IgG, decreased the percentages of CD8$^+$CD103$^+$ T cells in the forebrain of WNV-infected mice, without affecting the percentages of CD8$^+$ T cells. This suggests that the CXCL16/CXCR6 axis could be an important target to reduce T$_R$M cell differentiation without affecting CD8$^+$ trafficking into the CNS.

Conclusions

In summary, our studies identified unique, activated microglia clusters that persist in the CNS after recovery from viral encephalitis, with transcriptional signatures that suggest antigen-presenting capability or inflammatory function similar to those seen in aging and neurodegenerative diseases. We further identified CXCL16/CXCR6 factors as necessary for the maintenance of T$_R$M cells in the forebrain of mice during recovery from WNV infection, contributing to microglia and astrocyte activation, and synapse elimination in the CA3 region of the hippocampus. As initial activation of glial cells and infiltration of antiviral CD8$^+$ T cells into the CNS are critical for viral clearance, identification of mechanisms responsible for persistent neuroinflammation during recovery are essential for the development of successful therapeutics to prevent post-infectious cognitive sequelae without affecting viral clearance. The CXCL16/CXCR6 chemokine signaling pathway may also be an important target for other neurological and neurodegenerative diseases that are associated with neuroinflammation in the CNS.

Supplementary Information

The online version contains supplementary material available at https://doi.org/10.1186/s13073-022-01111-0.

Additional file 1: Table S1. Genes used to define cluster identity. **Table S2.** Top 25 defining genes for clusters 2 and 4. **Figure S1.** Split single cell clustering and nCount_RNA and nFeature_RNA plots. a. Split single cell clustering of the 4 biological samples processed for scRNA-sequencing. b. nCount_RNA and nFeature_RNA plots for cells that remained after QC. c. Representative gating strategy to identify live cells in mock and WNV-infected WT cortical and hippocampal samples (middle and right panel). A fluorescence minus one control (left panel) was also included. **Figure S2.** Pathway analysis of microglia clusters and tSNEs of microglia and T$_R$M markers. a. GO biological processes pathway analysis using generally applicable gene set enrichment (GAGE) method [36] based on the log2 fold changes from the single cell differential expression analysis. Pathway lists were generated with genes downregulated in Cluster 1 compared to Cluster 0 (top panel) and upregulated in Cluster 1 compared to Cluster 0 (bottom panel). b. Pathway lists were generated with genes downregulated in Cluster 3 compared to Cluster 1. No genes were significantly upregulated in Cluster 3 compared to Cluster 1. c. tSNE plots depicting the relative expression of microglial core genes, *P2ry12, Cx3cr1, Fcls, Siglech, Hexb,* and *Tmem119*. d. tSNE plots depicting the relative expression of T$_R$M genes, *Itgae, Cd44, Cd69,* and *Itga1*. Color key indicates the expression levels. **Figure S3.** Characterization of CXCR6$^+$CD4$^+$ and CD8$^+$ T cells during WNV infection. a, c. Flow cytometric analysis of the percent and number of CD4$^+$ T cells that are CXCR6$^+$ in the cortex (a) or hippocampus (c) of WNV-infected WT mice at 7, 25 and 52 DPI. b,d. Flow cytometric analysis of the number of CD8$^+$ T cells that are CXCR6$^+$ in the cortex (b) or hippocampus (d) of WNV-infected WT mice at 7, 25 and 52 DPI. e. Flow cytometric analysis of the percent of CXCR6$^+$ cells that are CD103$^+$NS4B$^-$ in the cortex (left) or hippocampus (right) of WNV-infected WT mice at 7, 25 and 52 DPI. f. Flow cytometric analysis of the percent of CD8$^+$ T cells that are IFNg$^+$ in the cortex and hippocampus of WNV-infected WT mice at 52 DPI. g. Flow cytometric analysis of the percent of CD4$^+$ T cells that are CXCR6$^+$ in the blood of WNV- infected mice at 7, 25 and 52 DPI. Data represent the mean±s.e.m. and were analyzed by unpaired Student's *t*-test. **Figure S4.** Characterization of *Cxcr6*$^{-/-}$ mice. a. Survival curve of WNV-infected *Cxcr6*$^{-/-}$ and WT mice. b. Weight loss

Rosen *et al. Genome Medicine*   (2022) 14:108

Page 18 of 20

course in WNV-infected *Cxcr6*^-/- and WT mice. c, d. Viral loads measured by plaque assay in the cortex (c) and hippocampus (d) of WNV-infected *Cxcr6*^-/- and WT mice at 7 or 12 DPI. e, f. Flow cytometric analysis of the percent of CD8$^+$CXCR6$^+$ and percent of CD4$^+$CXCR6$^+$ T cells in the cortex (e) and hippocampus (f) of WT and *Cxcr6*^-/- animals at 25 DPI. g. Flow cytometric analysis of the percent of CD8$^+$CD103$^+$ T cells that are NS4B$^+$ in the cortex and hippocampus of WNV-infected WT and *Cxcr6*^-/- at 7, 25, and 52 DPI. h,i. Flow cytometric analysis of the total number of CD4$^+$ T cells in the cortex (h) and hippocampus (i) of WT and *Cxcr6*^-/- animals at 7, 25 and 52 DPI. j. Flow cytometric analysis of the percent of CD45^{high} cells that are CD8$^+$, percent of CD8$^+$ cells that are NS4B$^+$ or CD103$^+$, and percent of CD45^{high} cells that are CD4$^+$ in the meninges of WNV-infected *Cxcr6*^-/- and WT mice at 25 and 52 DPI. k. Flow cytometric analysis of the percent of CD45^{high} cells that are CD8$^+$, percent of CD8$^+$ cells that are NS4B$^+$, and percent of CD45^{high} cells that are CD4$^+$ in the cervical lymph nodes (cLN) of WNV-infected *Cxcr6*^-/- and WT mice at 25 and 52 DPI. l. Flow cytometric analysis of the percent of CD45^{high} cells that are CD8$^+$ or CD4$^+$ in the blood of WNV-infected *Cxcr6*^-/- and WT mice at 7, 25 and 52 DPI. Data represent the mean±s.e.m. and were analyzed by unpaired Student's *t*-test. ****$P < 0.0001$. **Figure S5.** Analysis of T cell numbers in CXCR6-deficient animals. a,b. Flow cytometric analysis of total numbers of CD8$^+$, CD8$^+$CD103$^+$, and CD8$^+$NS4B$^+$ cells in the cortex and hippocampus of WT and *Cxcr6*^-/- mice at 7 (a) or 25 (b) DPI. Data represent the mean±s.e.m. and were analyzed by unpaired. **Figure S6.** Loss of CD8$^+$ T cells in the CNS is not due to T cell apoptosis, egression to the lymph node, or accumulation in the meninges in *Cxcr6*^-/- animals. a. Representative immunostaining and quantification of TUNEL (red), CD3 (green) and DAPI (blue) in CA3 region of the hippocampus of WNV-infected WT or *Cxcr6*^-/- mice at 25 and 52 DPI. Cell count quantified by counting of CD3$^+$TUNEL$^+$ cells per image and percentage quantified by number of CD3$^+$TUNEL$^+$ cells normalized to total CD3$^+$ cells. b. Flow cytometric analysis of the percentage of CD8$^+$ T cells that are CCR7$^+$ or CD62L$^+$ in the cortex, hippocampus, and lymph nodes at 35 DPI. Data represent the mean±s.e.m. and were analyzed by unpaired Student's t-testStudent's *t*-test. **Figure S7.** Gliosis persists in the hippocampus of WNV-infected WT and *Cxcr6*^-/- mice at 25 DPI. a. Representative immunostaining at 25 DPI of IL-1β (green), GFAP (red) and DAPI (blue) in CA3 region of the hippocampus of mock or WNV-infected WT or *Cxcr6*^-/- mice, followed by quantification of percent GFAP$^+$IL-1β$^+$ area, normalized to the total GFAP$^+$ area. **b.** Representative immunostaining at 25 DPI of IBA1 in mock- or WNV-infected WT or *Cxcr6*^-/- mice, showing staining for IBA1 (magenta) and DAPI (blue), followed by quantification of percent IBA1$^+$ area in the hippocampus. **c.** Representative immunostaining and quantification of synapses in the CA3 region of the hippocampus in mock- or WNV-infected WT or *Cxcr6*^-/- animals at 25 DPI showing staining for synaptophysin (red) and DAPI (blue). Synaptophysin quantified by percent positive area. Scale bars, 50 μm (a) or 20 μm (b,c). Data represent the mean±s.e.m. and were analyzed by two-way ANOVA and corrected for multiple comparisons. *$P<0.05$, **$P<0.005$, ****$P < 0.0001$. **Figure S8.** CXCL16 neutralization leads to decreased percentage and numbers of T$_R$M cells in the CNS at 15 and 25 DPI. a. Schematic depicting experimental design for CXCL16 neutralizing antibody experiment. Mice were infected (i.c.) with 1×10^4 p.f.u. WNV-NS5-E218A and administered CXCL16 antibody or isotype control via retro-orbital injection, and harvested 15 DPI. b. Quantification of percentage and number of CD8$^+$ cells that are CD103$^+$ in the cortex (left) and hippocampus (right) at 15 DPI in mice that received PBS or CXCL16 neutralizing antibody. c. Quantification of percentage and number of CD8$^+$ cells that are CD103$^+$ in the cortex (left) and hippocampus (right) at 25 DPI in mice that received PBS or CXCL16 neutralizing antibody. Data represent the mean±s.e.m. and were analyzed by unpaired Student's *t*-test. *$P<0.05$.

Availability of data and materials
The data from this study are tabulated in the main paper and an Additional file, which includes Tables S1 and S2, which list the genes used to define distinct clusters of CNS immune cells identified and the top 25 genes with the highest expression in clusters 2 and 4, respectively, and Figs. S1 (split single cell clustering and nCount_RNA and nFeature_RNA plots), S2 (pathway analysis of microglia clusters and tSNEs of microglia and T$_R$M markers), S3 (characterization of CXCR6$^+$CD4$^+$ and CD8$^+$ T cells during WNV infection), S4 (Characterization of *Cxcr6*$^{-/-}$ mice), S5 (analysis of T cell numbers in CXCR6-deficient animals), S6 (loss of CD8$^+$ T cells in the CNS is not due to T cell apoptosis, egression to the lymph node, or accumulation in the meninges in *Cxcr6*$^{-/-}$ animals), S7 (gliosis persists in the hippocampus of WNV-infected WT and *Cxcr6*$^{-/-}$ mice at 25 DPI), and S8 (CXCL16 neutralization leads to decreased percentage and numbers of T$_R$M cells in the CNS at 15 and 25 DPI). All non-commercially reagents are available upon request via email from R.S.K. under a material transfer agreement with Washington University. The scRNA-seq data discussed in this publication have been deposited in NCBI's Gene Expression Omnibus and are accessible through GEO Series accession number GSE212199 [69].

Declarations

Ethics approval and consent to participate
All murine experiments followed guidelines approved by the Washington University School of Medicine Animals Safety Committee (Animal Welfare Assurance # A-3381-01 protocol no. 20180120).

Consent for publication
Not applicable

Competing interests
The authors declare that they have no competing interests.

Author details
[1]Center for Neuroimmunology and Neuroinfectious Diseases, Washington University School of Medicine, St. Louis, MO, USA. [2]Department of Internal Medicine, Washington University School of Medicine, St. Louis, MO, USA. [3]Department of Genetics, Washington University School of Medicine, St. Louis, MO, USA. [4]Department of Pathology and Immunology, Washington University School of Medicine, St. Louis, MO, USA. [5]Department of Pediatrics, Washington University School of Medicine, St. Louis, MO, USA. [6]Department of Neuroscience, Washington University School of Medicine, St. Louis, MO, USA.

References
1. Centers for Disease Control and Prevention (CDC). West Nile virus disease and other arboviral diseases - United States, 2011. MMWR Morb Mortal Wkly Rep. 2012;61(27):510–4 http://www.ncbi.nlm.nih.gov/pubmed/22785342. Accessed 21 Sept 2018.
2. Shrestha B, Samuel MA, Diamond MS. CD8 + T cells require perforin to clear West Nile virus from infected neurons. J Virol. 2006;80(1):119–29. https://doi.org/10.1128/JVI.80.1.119-129.2006.
3. Szretter KJ, Daniels BP, Cho H, et al. 2′-O methylation of the viral mRNA cap by West Nile virus evades Ifit1-dependent and -independent

mechanisms of host restriction in vivo. PLoS Pathog. 2012;8(5). https://doi.org/10.1371/JOURNAL.PPAT.1002698.

4.   Aguilar-Valenzuela R, Netland J, Seo Y-J, Bevan MJ, Grakoui A, Suthar MS. Dynamics of tissue-specific CD8 $^+$ T cell responses during West Nile virus infection. Dutch RE, ed. J Virol. 2018;92(10):e00014–8. https://doi.org/10.1128/JVI.00014-18.

5.   Murray KO, Garcia MN, Rahbar MH, et al. Survival analysis, long-term outcomes, and percentage of recovery up to 8 years post-infection among the Houston West Nile virus cohort. Baldanti F, ed. PLoS One. 2014;9(7):e102953. https://doi.org/10.1371/journal.pone.0102953.

6.   He J, Yamada K, Nabeshima T. A role of Fos expression in the CA3 region of the hippocampus in spatial memory formation in rats. Neuropsychopharmacol. 2002;26(2):259–68. https://doi.org/10.1016/s0893-133x(01)00332-3.

7.   RGM Morris PGJRJO. Place navigation in rats with hippocampal lesions. Nature. 1982;297(5868):681–3. https://doi.org/10.1038/297681a0.

8.   Zhao W, SCPGDA. Nonreceptor tyrosine protein kinase pp60c-src in spatial learning: synapse-specific changes in its gene expression, tyrosine phosphorylation, and protein-protein interactions. Proc Natl Acad Sci USA. 2000;97(14):8098–103. https://doi.org/10.1073/pnas.97.14.8098.

9.   Vasek MJ, Garber C, Dorsey D, et al. A complement–microglial axis drives synapse loss during virus-induced memory impairment. Nature. 2016;534(7608):538–43. https://doi.org/10.1038/nature18283.

10. Garber C, Soung A, Vollmer LL, et al. T cells promote microglia-mediated synaptic elimination and cognitive dysfunction during recovery from neuropathogenic flaviviruses. Nat Neurosci. 2019;22(8). https://doi.org/10.1038/s41593-019-0427-y.

11. Masuda T, Sankowski R, Staszewski O, Prinz M. Microglia heterogeneity in the single-cell era. Cell Rep. 2020;30(5):1271–81. https://doi.org/10.1016/J.CELREP.2020.01.010.

12. Ajami B, Samusik N, Wieghofer P, et al. Single-cell mass cytometry reveals distinct populations of brain myeloid cells in mouse neuroinflammation and neurodegeneration models. Nat Neurosci. 2018;21(4):541–51. https://doi.org/10.1038/S41593-018-0100-X.

13. Srinivasan K, Friedman BA, Etxeberria A, et al. Alzheimer's patient microglia exhibit enhanced aging and unique transcriptional activation. Cell Rep. 2020;31(13). https://doi.org/10.1016/j.celrep.2020.107843.

14. Krasemann S, Madore C, Cialic R, et al. The TREM2-APOE pathway drives the transcriptional phenotype of dysfunctional microglia in neurodegenerative diseases. Immunity. 2017;47(3):566–581.e9. https://doi.org/10.1016/J.IMMUNI.2017.08.008.

15. Luther SA, Cyster JG. Chemokines as regulators of T cell differentiation. Nat Immunol. 2001;2(2):102–7. https://doi.org/10.1038/84205.

16. Rahimi RA, Luster AD. Chemokines: critical regulators of memory T cell development, maintenance, and function. Adv Immunol. 2018;138:71–98. https://doi.org/10.1016/BS.AI.2018.02.002.

17. Matloubian M, David A, Engel S, Ryan JE, Cyster JG. A transmembrane CXC chemokine is a ligand for HIV-coreceptor Bonzo. Nat Immunol. 2000;1(4):298–304. https://doi.org/10.1038/79738.

18. Abel S, Hundhausen C, Mentlein R, et al. The transmembrane CXC-chemokine ligand 16 is induced by IFN-γ and TNF-α and shed by the activity of the disintegrin-like metalloproteinase ADAM10. J Immunol. 2004;172(10):6362–72. https://doi.org/10.4049/jimmunol.172.10.6362.

19. Ludwig A. Enhanced expression and shedding of the transmembrane chemokine CXCL16 by reactive astrocytes and glioma cells. J Neurochem. 2005;93:1293–303.

20. Ludwig A, RM. Glial cross-talk by transmembrane chemokines CX3CL1 and CXCL16. J Neuroimmunol. 2008;198:92–7.

21. Lepore F, D'Alessandro G, Antonangeli F, et al. CXCL16/CXCR6 axis drives microglia/macrophages phenotype in physiological conditions and plays a crucial role in glioma. Front Immunol. 2018;9(NOV):2750. https://doi.org/10.3389/fimmu.2018.02750.

22. Rosito M, Deflorio C, Limatola C, Trettel F. CXCL16 orchestrates adenosine A 3 receptor and MCP-1/CCL2 activity to protect neurons from excitotoxic cell death in the CNS. J Neurosci. 2012;32(9):3154–63. https://doi.org/10.1523/JNEUROSCI.4046-11.2012.

23. Li G, KHRMHMJH-F. The transmembrane chemokines CXCL16 and CX3CL1 and their receptors are expressed in human meningiomas. Oncol Rep. 2013;29:563–70.

24. Held-Feindt J. Overexpression of CXCL16 and its receptor CXCR6/Bonzo promotes growth of human schwannomas. Glia. 2008;56:764–74.

25. Lambert JC, Ibrahim-Verbaas CA, Harold D, et al. Meta-analysis of 74,046 individuals identifies 11 new susceptibility loci for Alzheimer's disease. Nat Genet. 2013;45(12):1452–8. https://doi.org/10.1038/ng.2802.

26. Tse S-W, Radtke AJ, Espinosa DA, Cockburn IA, Zavala F. The chemokine receptor CXCR6 is required for the maintenance of liver memory CD8+ T cells specific for infectious pathogens. J Infect Dis. 2014;210(9):1508–16. https://doi.org/10.1093/infdis/jiu281.

27. Wein AN, McMaster SR, Takamura S, et al. CXCR6 regulates localization of tissue-resident memory CD8 T cells to the airways. J Exp Med. 2019;216(12):2748–62. https://doi.org/10.1084/jem.20181308.

28. Sato T, Thorlacius H, Johnston B, et al. Role for CXCR6 in recruitment of activated CD8 + lymphocytes to inflamed liver. J Immunol. 2005;174(1):277–83. https://doi.org/10.4049/jimmunol.174.1.277.

29. Smolders J, Heutinck KM, Fransen NL, et al. Tissue-resident memory T cells populate the human brain. Nat Commun. 2018;9(1). https://doi.org/10.1038/S41467-018-07053-9.

30. Alves de Lima K, Rustenhoven J, Da Mesquita S, et al. Meningeal γδ T cells regulate anxiety-like behavior via IL-17a signaling in neurons. Nat Immunol. 2020;21(11):1421–9. https://doi.org/10.1038/s41590-020-0776-4.

31. Zhang Y. An RNA-sequencing transcriptome and splicing database of glia, neurons, and vascular cells of the cerebral cortex. J Neurosci. 2014;34:11929–47.

32. DePaula-Silva AB, Gorbea C, Doty DJ, et al. Differential transcriptional profiles identify microglial- and macrophage-specific gene markers expressed during virus-induced neuroinflammation. J Neuroinflammation. 2019;16(1):1–20. https://doi.org/10.1186/S12974-019-1545-X.

33. Stratoulias V, Venero JL, Tremblay M-È, Joseph B. Microglial subtypes: diversity within the microglial community. EMBO J. 2019;38(17):e101997. https://doi.org/10.15252/EMBJ.2019101997.

34. Pan J, Ma N, Yu B, Zhang W, Wan J. Transcriptomic profiling of microglia and astrocytes throughout aging. J Neuroinflammation. 2020;17(1):1–19. https://doi.org/10.1186/S12974-020-01774-9.

35. Jurga AM, Paleczna M, Kuter KZ. Overview of general and discriminating markers of differential microglia phenotypes. Front Cell Neurosci. 2020;0:198. https://doi.org/10.3389/FNCEL.2020.00198.

36. Luo W, Friedman MS, Shedden K, Hankenson KD, Woolf PJ. GAGE: generally applicable gene set enrichment for pathway analysis. BMC Bioinforma. 2009;10(1):1–17. https://doi.org/10.1186/1471-2105-10-161.

37. Mattei D, Ivanov A, van Oostrum M, et al. Enzymatic dissociation induces transcriptional and proteotype bias in brain cell populations. Int J Mol Sci. 2020;21(21):1–20. https://doi.org/10.3390/IJMS21217944.

38. Marsh SE, Walker AJ, Kamath T, et al. Dissection of artifactual and confounding glial signatures by single-cell sequencing of mouse and human brain. Nat Neurosci. 2022;25(3):306–16. https://doi.org/10.1038/s41593-022-01022-8.

39. Ellwardt E, Walsh JT, Kipnis J, Zipp F. Understanding the role of T cells in CNS homeostasis. Trends Immunol. 2016;37(2):154–65. https://doi.org/10.1016/J.IT.2015.12.008.

40. Li Q. Developmental heterogeneity of microglia and brain myeloid cells revealed by deep single-cell RNA sequencing. Neuron. 2019;101:207–23.

41. Haimon Z, Volaski A, Orthgiess J, et al. Re-evaluating microglia expression profiles using RiboTag and cell isolation strategies. Nat Immunol. 2018;19(6):636–44. https://doi.org/10.1038/S41590-018-0110-6.

42. Li Q, BB. Microglia and macrophages in brain homeostasis and disease. Nat Rev Immunol. 2018;18:225–42.

43. Butovsky O, Weiner HL. Microglial signatures and their role in health and disease. Nat Rev Neurosci. 2018;19(10):622–35. https://doi.org/10.1038/S41583-018-0057-5.

44. Swanson MEV, Scotter EL, Smyth LCD, et al. Identification of a dysfunctional microglial population in human Alzheimer's disease cortex using novel single-cell histology image analysis. Acta Neuropathol Commun. 2020;8(1):1–16. https://doi.org/10.1186/S40478-020-01047-9.

45. Kreutzfeldt M, Bergthaler A, Fernandez M, et al. Neuroprotective intervention by interferon-γ blockade prevents CD8+ T cell-mediated dendrite and synapse loss. J Exp Med. 2013;210(10):2087–103. https://doi.org/10.1084/jem.20122143.

46. Klein R, Lin E, Zhang B, Luster A, Tollett J. Neuronal CXCL10 directs CD8+ T cell recruitment and control of West Nile virus encephalitis. J Virol. 2005;79.

47. Zhang B, Patel J, Croyle M, Diamond MS, Klein RS. TNF-α-dependent regulation of CXCR3 expression modulates neuronal survival during

Rosen *et al. Genome Medicine*   (2022) 14:108

Page 20 of 20

West Nile virus encephalitis. J Neuroimmunol. 2010;224(1-2):28–38. https://doi.org/10.1016/J.JNEUROIM.2010.05.003.

48. Durrant DM, Daniels BP, Klein RS. IL-1R1 signaling regulates CXCL12-mediated T cell localization and fate within the central nervous system during West Nile virus encephalitis. J Immunol. 2014;193(8):4095–106. https://doi.org/10.4049/jimmunol.1401192.

49. Zhang B, Chan Y, Lu B, Diamond M, Klein R. CXCR3 mediates region-specific antiviral T cell trafficking within the central nervous system during West Nile virus encephalitis. J Immunol. 2008;180.

50. Kaabinejadian S, McMurtrey CP, Kim S, et al. Immunodominant West Nile virus T cell epitopes are fewer in number and fashionably late. J Immunol. 2016;196(10):4263–73. https://doi.org/10.4049/JIMMUNOL.1501821.

51. Weninger W, Crowley MA, Manjunath N, von Andrian UH. Migratory properties of naive, effector, and memory CD8(+) T cells. J Exp Med. 2001;194(7):953–66. https://doi.org/10.1084/JEM.194.7.953.

52. Bromley SK, Thomas SY, Luster AD. Chemokine receptor CCR7 guides T cell exit from peripheral tissues and entry into afferent lymphatics. Nat Immunol. 2005;6(9):895–901. https://doi.org/10.1038/NI1240.

53. Garber C, Vasek MJ, Vollmer LL, Sun T, Jiang X, Klein RS. Astrocytes decrease adult neurogenesis during virus-induced memory dysfunction via IL-1. Nat Immunol. 2018;19(2):151–61. https://doi.org/10.1038/s41590-017-0021-y.

54. Mackay LK, Rahimpour A, Ma JZ, et al. The developmental pathway for CD103+CD8+ tissue-resident memory T cells of skin. Nat Immunol. 2013;14(12):1294–301. https://doi.org/10.1038/ni.2744.

55. Lim SM, Koraka P, Osterhaus ADME, Martina BEE. West Nile virus: immunity and pathogenesis. Viruses. 2011;3(6):811–28. https://doi.org/10.3390/v3060811.

56. Klein RS, Garber C, Funk KE, et al. Neuroinflammation during RNA viral infections. Annu Rev Immunol. 2019;37:73–95. https://doi.org/10.1146/annurev-immunol-042718-041417.

57. Armand EJ, Li J, Xie F, Luo C, Mukamel EA. Single-cell sequencing of brain cell transcriptomes and epigenomes. Neuron. 2021;109(1):11–26. https://doi.org/10.1016/J.NEURON.2020.12.010.

58. Silvin A, Ginhoux F. Microglia heterogeneity along a spatio–temporal axis: more questions than answers. Glia. 2018;66(10):2045–57. https://doi.org/10.1002/glia.23458.

59. Masuda T, Prinz M. Microglia: a unique versatile cell in the central nervous system. ACS Chem Neurosci. 2016;7(4):428–34. https://doi.org/10.1021/ACSCHEMNEURO.5B00317.

60. Dubbelaar ML, Kracht L, Eggen BJL, Boddeke EWGM. The kaleidoscope of microglial phenotypes. Front Immunol. 2018;9:1753. https://doi.org/10.3389/FIMMU.2018.01753.

61. Butovsky O, Jedrychowski MP, Moore CS, et al. Identification of a unique TGF-β–dependent molecular and functional signature in microglia. Nat Neurosci. 2014;17(1):131–43. https://doi.org/10.1038/nn.3599.

62. Belloy ME, Napolioni V, Greicius MD. A quarter century of APOE and Alzheimer's disease: progress to date and the path forward. Neuron. 2019;101(5):820–38. https://doi.org/10.1016/J.NEURON.2019.01.056.

63. Smith LK, He Y, Park J-S, et al. β2-microglobulin is a systemic pro-aging factor that impairs cognitive function and neurogenesis. Nat Med. 2015;21(8):932. https://doi.org/10.1038/NM.3898.

64. Fukumoto N, Shimaoka T, Fujimura H, et al. Critical roles of CXC chemokine ligand 16/scavenger receptor that binds phosphatidylserine and oxidized lipoprotein in the pathogenesis of both acute and adoptive transfer experimental autoimmune encephalomyelitis. J Immunol. 2004;173(3):1620–7. https://doi.org/10.4049/jimmunol.173.3.1620.

65. Wakim LM, Woodward-Davis A, Bevan MJ. Memory T cells persisting within the brain after local infection show functional adaptations to their tissue of residence. Proc Natl Acad Sci U S A. 2010;107(42):17872–9. https://doi.org/10.1073/pnas.1010201107.

66. Zaid A, Hor JL, Christo SN, et al. Chemokine receptor–dependent control of skin tissue–resident memory T cell formation. J Immunol. 2017;199(7):2451–9. https://doi.org/10.4049/JIMMUNOL.1700571.

67. Ashhurst AS, Flórido M, Lin LCW, et al. CXCR6-deficiency improves the control of pulmonary mycobacterium tuberculosis and influenza infection independent of T-lymphocyte recruitment to the lungs. Front Immunol. 2019;10(MAR). https://doi.org/10.3389/FIMMU.2019.00339/FULL.

68. Ai S, Klein RS. Update on T cells in the virally infected brain: friends and foes. Curr Opin Neurol. 2020;33(3):405–12. https://doi.org/10.1097/WCO.0000000000000825.

69. Rosen SF, Soung AL, Yang W, Ai S, Kanmogne M, Dave VA, Artyomov M, Magee JA, Klein RS. Single-cell RNA transcriptome analysis of CNS immune cells reveals CXCL16/CXCR6 as maintenance factors for tissue resident T cells that drive synapse elimination. Gene Expression Omnibus/NCBI Accession GSE212199. https://www.ncbi.nlm.nih.gov/geo/query/acc.cgi?acc=GSE212199

Publisher's Note